Stony Brook University

The official electronic file of this thesis or dissertation is maintained by the University Libraries on behalf of The Graduate School at Stony Brook University.

Higher-Order Modes in the BNL Energy Recovery Linac: Measurement and Waveguide Coupler Design

A Thesis Presented

by

Elliott Curtis Johnson

to

The Graduate School

in Partial Fulfillment of the Requirements

for the Degree of

Master of Science

in

Physics

(Scientific Instrumentation)

Stony Brook University

December 2011

Stony Brook University

The Graduate School

Elliott Curtis Johnson

We, the thesis committee for the above candidate for the Master of Science degree, hereby recommend acceptance of this thesis.

Ilan Ben-Zvi – Thesis Advisor
BNL Professor, Department of Physics and Astronomy
Stony Brook University

Xu Du
Assistant Professor, Department of Physics and Astronomy
Stony Brook University

Peter M. Koch
Professor, Department of Physics and Astronomy
Stony Brook University

Dmitri Tsybychev
Assistant Professor, Department of Physics and Astronomy
Stony Brook University

This thesis is accepted by the Graduate School.

Lawrence Martin
Dean of the Graduate School

Abstract of the Thesis

Higher-Order Modes in the BNL Energy Recovery Linac: Measurement and Waveguide Coupler Design

by

Elliott Curtis Johnson

Master of Science

in

Physics

(Scientific Instrumentation)

Stony Brook University

2011

As in many resonators, higher-order modes (HOMs) occur in particle accelerator radio frequency (RF) cavities. The excitation of these harmonics causes additional heat loads in cryogenic systems and can result in problematic single bunch and multi-bunch effects. It is therefore critical to understand HOM prevalence and structure, and devise a method of extracting their power from the accelerator cavity. Research on these topics is ongoing in the Collider-Accelerator Dept. at Brookhaven National Laboratory (BNL), where the construction of an Energy Recovery Linac is underway. An HOM coupler implementing a dual-ridge waveguide has been designed for use on the next-generation ERL cavity. A full description of the design from its early stages is given, along with simulated analysis of its performance. Also, to better understand resonances occurring in the existing ERL, a measurement

routine was developed to characterize and identify HOMs using a bead-pulling technique on a copper prototype cavity. Initial results of these measurements show a good correspondence with the harmonics predicted by the simulation code CST Microwave Studio.

Dedicated to my family.

Contents

List of Figures

List of Tables

Acknowledgements

This work results from the efforts of many colleagues and collaborators, particularly those within the Collider-Accelerator Dept. at BNL.

My advisor, Ilan Ben-Zvi, possesses a vast knowledge of accelerator physics and superconducting RF science, a broad vision for the state-of-the-art of those fields, and a strong sense of leadership. His generosity and graciousness as a mentor provided guidance in the trials of both science and life. For these reasons it has been a great honor to study under his direction.

Wencan Xu, my friend and colleague, has provided endless support and careful attention to my research. His help with many of the setbacks I faced – troubleshooting computational errors, understanding physical principles, or deciding how to approach the next problem – is unreservedly appreciated. Moreover, I've been truly inspired by his modesty and the high level of integrity with which he conducts his scientific work.

I wish to thank Harald Hahn for his vital contributions to the higher-order mode measurement and analysis efforts. His insight and curiosity provided much of the motivation and direction to this research.

I've benefited greatly from discussions with many other C-AD employees, past and present, including Steve Bellavia, Sergey Belomestnykh, Nathan Cook, Lee Hammons, Puneet Jain, Vladimir Litvinenko, Todd Satogata, Stephen Webb, and Qiong Wu. The research contained in these pages could not have been concluded without all their contributions.

Lastly, I'd like to give a special acknowledgement to Hal Metcalf, my graduate program director, for dutifully running a successful program and taking an active interest in my progress along the way.

ELLIOTT C. JOHNSON
Upton, NY
December 2011

Chapter 1

Introduction

This chapter gives a brief background of the energy recovery linac effort at BNL and describes a next-generation 5-cell cavity design being constructed for an envisioned electron-ion collider. Also covered is the basic science of HOMs in accelerator cavities: their physical origin, analysis by computational simulation, and three methods used to extract their power from accelerators.

1.1 Energy Recovery Linac at BNL

An energy recovery linac (ERL) is a multi-pass accelerator that recirculates high-energy electrons out of phase in order to recover their energy with a high efficiency. Currently, an ampere-class superconducting ERL is under construction at the Collider-Accelerator Department at BNL. It is comprised of a 5-cell radio frequency (RF) cavity (denoted "BNL1") and photo-injector RF electron gun, both operating at 703.75 MHz[1, 2]. The facility is a proof-of-principle program serving as a test-bed for upgrades in the Relativistic Heavy Ion Collider (RHIC) aimed at eRHIC (colliding electrons with RHIC ions) and electron cooling. Both upgrades require good quality, high-current electron beams from ERLs. A schematic of the BNL ERL is given in Fig. 1.1 [3].

1.1.1 Current Status

At the time of this writing, the full ERL ring isn't complete; however, the 5-cell superconducting cavity and cryostat are in place. Additionally, a copper prototype version of the BNL1 cavity is available for room temperature study. Such prototypes allow a great opportunity for HOM measurement, including bead-pulling, which is the topic of Chapter 4.
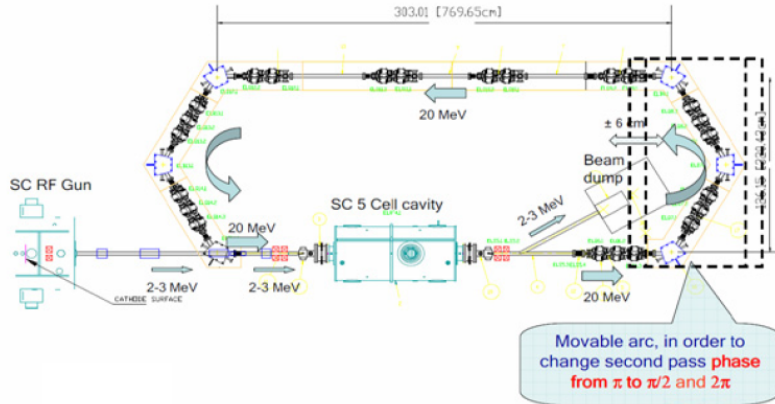
Figure 1.1: *Schematic of the ERL at BNL.*

1.1.2 ERL 5-cell Cavity Design Upgrade

In addition to the current R&D ERL under construction, a next-generation 5-cell cavity (termed "BNL3") has been designed and optimized[4]. BNL3 is intended to satisfy beam requirements for the next iteration of ERL testing at BNL as part of an envisioned future electron-ion collider, eRHIC. The cavity's optimized geometry features a much-improved ratio of shunt impedance R to Q for the fundamental accelerating mode, a quantity that determines the degree to which a particle in the beam will be accelerated by the field. At the same time, the BNL3 cavity features decreased $\frac{R}{Q} \cdot Q$ values for HOMs, which are detrimental to beam operation.

More information on HOMs is given in subsequent sections of this chapter, including 3 damping methods used to reduce their harmful effects in accelerator cavities: ferrite, coaxial filter, and waveguide couplers. While a coax filter coupler design has been completed for BNL3, the prototype BNL3 cavity will feature detachable beam tubes, allowing for R&D of other damping designs. Chapters 2-3 describe an HOM damper utilizing a dual-ridge WG suitable for high-current accelerators.

1.2 Higher-Order Modes

As in most resonators, accelerator cavities allow the occurrence of modes with propagation constants and electromagnetic field distributions different from the design (or "fundamental") mode. In accelerators, these modes generally occur at higher frequencies than the fundamental, and are thus called higher-order modes. The fundamental mode has a longitudinal E-field along the cavity axis, which transfers energy in the RF field to kinetic energy in the

particle bunch. However, the converse situation may also occur: a charge bunch passing through an accelerator cavity can excite HOMs, possibly with strong off-axis fields. These high-frequency resonances are detrimental to accelerator operation because they are a source of beam instabilities, and, in extreme cases, complete beam loss – a condition known as beam break-up (BBU). In superconducting systems, HOMs also result in additional cryogenic losses due to excessive power dissipation in cavity walls. To avoid these concerns, successful damping of HOMs is a critical requirement of accelerators.

The effects of HOMs are gradually becoming more of a concern in modern accelerators, which feature larger currents and bunch charges than previous installations.[1] The average HOM power is given by

$$P_{avg} = k_l Q I \tag{1.1}$$

where k_l is the cavity loss factor, Q is the bunch charge, and I is the beam current, in turn calculated by

$$I = n F_{bunch} Q. \tag{1.2}$$

In the above equation, n is the number of passes and F_{bunch} is the bunch frequency. For the eRHIC parameters (3.6 nC bunches through 6 accelerating and 6 decelerating passes at 9.4 MHz bunch frequency), this leads to HOM power of nearly 8 kW per cavity.

The electric and magnetic field distributions for HOMs are determined by the cavity geometry. In the accelerator community, the traditional way of classifying modes in a cylindrical oscillator is TM_{mnp} (for transverse-magnetic modes) or TE_{mnp} (for transverse-electric) where m,n, and p denote the number of sign changes in the ϕ, ρ, and z directions, respectively. For example, the fundamental mode is a TM_{010} mode. Furthermore, a common vocabulary used to classify HOMs is by their m value – "monopole" ($m = 0$), "dipole" ($m = 1$), "quadrupole" ($m = 2$), etc. The names are derived from the shape of the cross-sectional field profile. Examples of some of these HOM field patterns are given in Fig. 1.2.

Dipole modes are particularly hazardous in accelerators because they're more easily excited due to their linear field nature near the beam center. An explanation of an important figure of merit, the quality factor, and the relation between energy loss and this quantity for a dipole HOM are given in the next sections.

---

[1]To this end, a dedicated workshop "HOM10" was recently held at Cornell University – see http://lepp.cornell.edu/Events/HOM10/WebHome.html
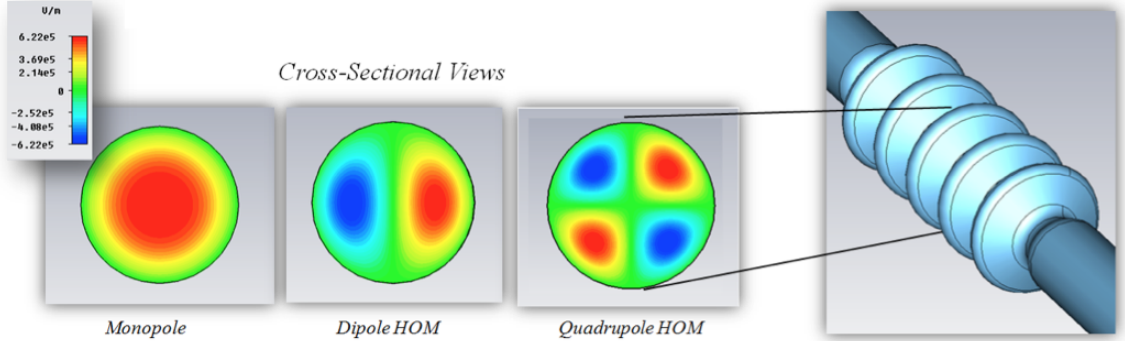
Figure 1.2: *Cross sectional views of the fundamental mode and selected HOMs in the BNL1 cavity. The colored sections indicate longitudinal electric fields generated by CST Microwave Studio (blue and red sections are opposite in phase).*

1.2.1 Quality Factor

As described by Padamsee[5], the quality factor for an accelerator cavity is defined as

$$Q_0 = \frac{\omega U}{P_c},$$ (1.3)

where U is the stored energy in the cavity, P_c is the power dissipated in the cavity walls, and ω is the frequency of the accelerating mode. Q_0 is directly measured with a network analyzer as the ratio of center frequency to resonance width 3 dB below the peak. This is the accepted convention of the accelerator community.

When incident or outgoing power couplers are attached to the cavity, analogous quality factors can be assigned. For example, when considering the power transferred back out of the input coupler (P_e) and power passing through the transmitted power coupler (P_t), The quality factor is now referred to as "loaded Q", or Q_L:

$$Q_L = \frac{\omega U}{P_{tot}},$$ (1.4)

for

$$P_{tot} = P_c + P_e + P_t.$$ (1.5)

In a similar way, "external Q" (Q_{ext}), for which only the power transferred out of a transmitted coupler is considered, can be defined. More discussion about Q_{ext} is given in section 1.3.1.

4

1.2.2 Energy Loss to a Dipole Mode

The energy lost by a charge to a dipole mode is given by the 15th chapter of Padamsee[5]:

$$U_q = k_d q^2 \left(\frac{\rho}{a}\right)^2 \tag{1.6}$$

where q is the elementary charge, a is the beam tube radius, ρ is the distance off axis, and k_d is the loss factor, which is directly related to a mode's "R over Q":

$$k_d = a^2 \left(\frac{\omega_n}{c}\right)^2 \frac{\omega_n}{4} \frac{R_{sh}}{Q_0}, \tag{1.7}$$

Here ω_n is the mode's eigenfrequency, c is the speed of light, R_{sh} is the shunt impedance, and Q_0 is the quality factor. The value for $\frac{R_{sh}}{Q_0}$ is found from simulation (see next section). The product of $\frac{R_{sh}}{Q_0}$ and Q_0 is shunt impedance, a quantity which must be limited for beam stability. For example, Fig. 1.3 shows measured Q values for HOMs in the ERL, along with the maximum stable Q of these modes[3]. As evident by a gradual upward trend in the figure, the BBU limit depends inversely on frequency. The code CST Microwave Studio, used to estimate stable Q, assumes the modes are dipoles and a beam current of 0.5 A. This code is described in the following section.
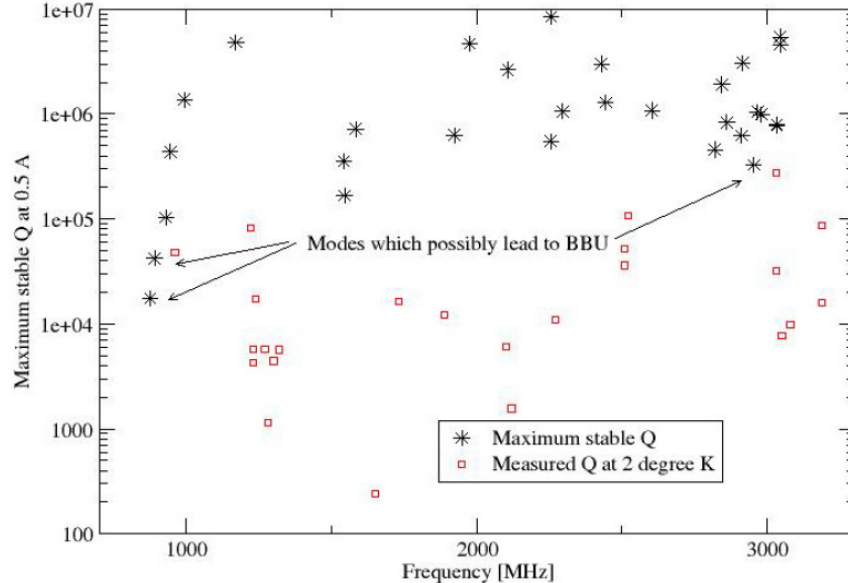
Figure 1.3: *The maximum stable Q of dipole HOMs for the R&D ERL, calculated from MWS and Q values measured at 2 K.*

1.2.3   HOM Simulation with CST Microwave Studio

One of the codes in use by the Collider-Accelerator Department at BNL for electromagnetic analysis of accelerator components is CST Microwave Studio (MWS)[6]. This software employs a 3-dimensional CAD interface along with several different solvers, including eigenmode, transient, and frequency domain. The eigenmode solver is used to analyze HOMs, by outputting their frequency, field profiles, and $\frac{R}{Q}$ values. Fig. 1.4 shows the MWS model of the BNL3 cavity, and Fig. 1.5 shows a graphical output of a BNL1 dipole HOM found by the eigenmode solver. The field distributions for an HOM eigenmode solutions in MWS can be used to construct a correspondence between simulation results and HOMs measured in the lab.
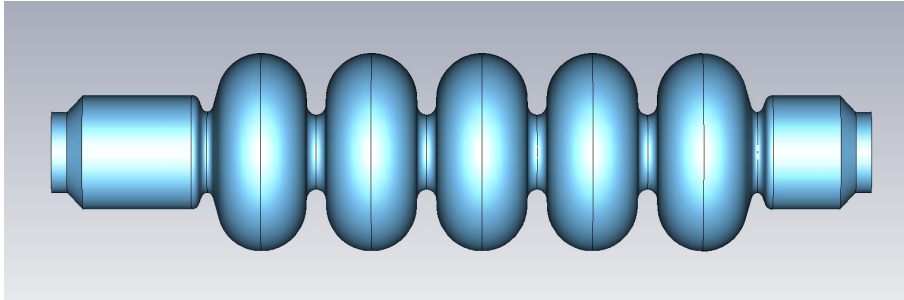
Figure 1.4: *MWS model of the BNL3 cavity.*
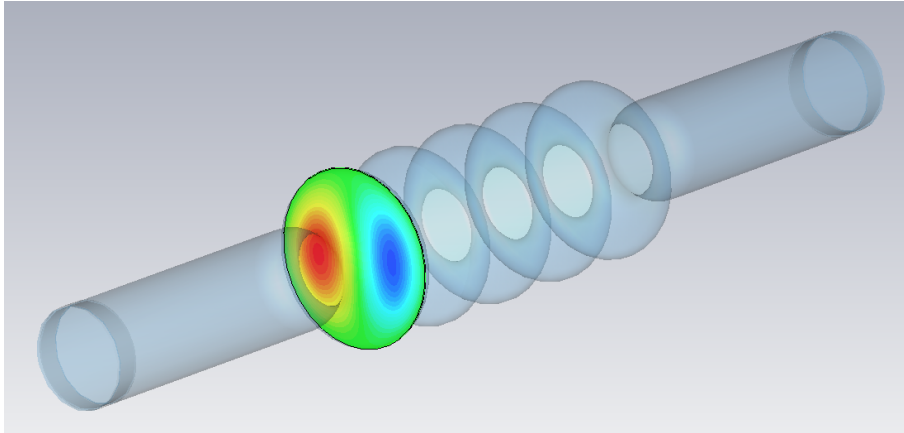
Figure 1.5: *A MWS dipole mode result in the BNL1 cavity. A cross-sectional slice of the longitudinal E-field is shown.*

1.2.4 HOM Measurement

To determine the correspondence between modes found by the MWS solver and those actually occurring in the lab, cavity resonances can also be measured using multiple techniques. The locations and Q-values for all modes are easily seen by spikes in the transmission when a network analyzer is used in transmission mode to measure S_{21}, which is related to incident and outgoing power by

$$S_{21}(dB) = 10 \cdot \log_{10}\left(\frac{P_{out}}{P_{in}}\right).\tag{1.8}$$

Such a measurement is shown for the niobium BNL1 cavity in Fig. 1.6. However, actually identifying an HOM (as a dipole, quadrupole, etc.) takes more effort. One successful method using capacitive probes in holes drilled in copper BNL1 cavity cells has been used to study HOMs in the ERL[7]. Another technique, bead-pulling, involves measuring the shift in phase (or amplitude) of a resonance as a small perturbation is moved through the cavity (such as a conducting bead on a string). A bead-pulling assembly was constructed on the copper BNL1 cavity, and a thorough description of the setup and measurements is given in Chapter 4.

1.3 Higher-Order Mode Couplers

For successful beam operation, HOM power must be removed from the accelerator, and this is accomplished through the use of HOM couplers (or "dampers") – devices with 2 basic requirements: providing a pathway for high-frequency power out of the accelerator while simultaneously rejecting signals at the fundamental accelerating frequency. The next sections relate the HOM power to relevant cavity parameters and describe common HOM coupler designs.

1.3.1 HOM Power

The HOM power P transmitted into an HOM coupler is related to a the external Q (calculated with MWS) by

$$P = \frac{\omega U}{Q_{ext}},\tag{1.9}$$

where the numerator can be replaced by the accelerating voltage V and $\frac{R}{Q}$ as shown by Padamsee (2.66):
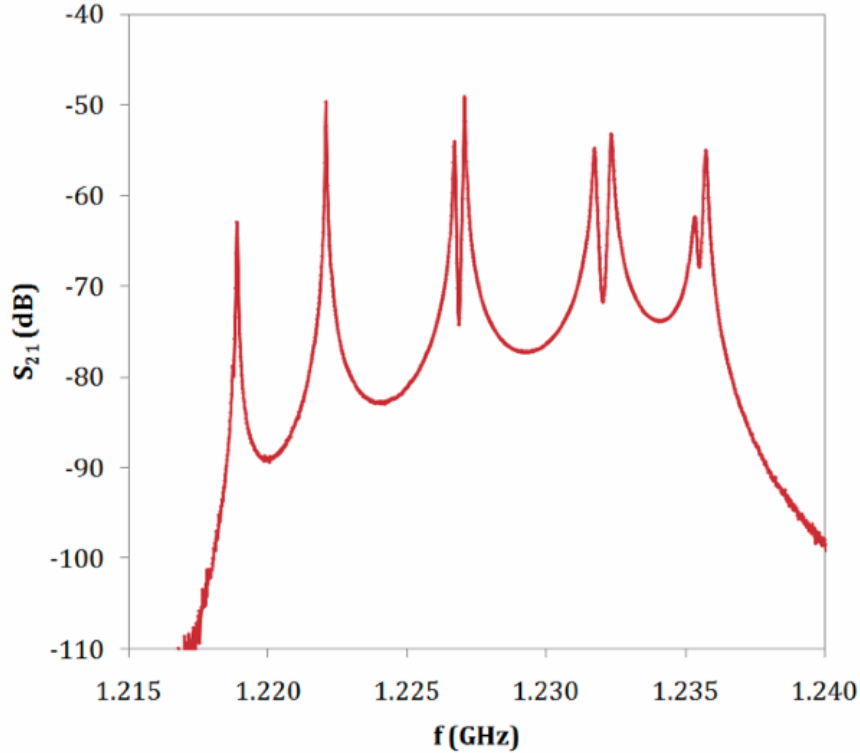
Figure 1.6: S_{21} *as measured in the copper BNL1 cavity, showing a family of HOM resonances. Some of the modes exhibit "splitting" from 2 polarizations of the modes being excited due to cavity geometry imperfections.*

$$\omega U = \frac{V^2}{\frac{R}{Q}}.\tag{1.10}$$

Using these equations, the power coupled out of the accelerator cavity for each HOM can be estimated by simulation.

1.3.2 HOM Coupler Types

The BNL1 cavity design includes beam tubes attached to each end of the 5-cell cavity, with a cutoff diameter chosen to restrict propagation of only the lowest-frequency, fundamental mode at 703.75 MHz[1]. Since the fields for HOMs (but not the fundamental mode) are highly prevalent in the beam tubes, this region is an ideal location to couple HOM power out of the resonator without affecting the accelerating fields or disturbing the cavity geometry. Furthermore, the end cells in the cavity were designed with a slight asymmetry to decrease the likelihood of so-called "trapped" modes – HOMs with fields that do not

8

extend into the beam tubes. This design strategy is common in many modern accelerator structures.

There are several different types of HOM dampers, and 3 common designs are described below. A more thorough discussion of these is given in Chapter 16 of Padamsee[5].

Ferrite Absorbers

Ferrite dampers consist of a rings of ferromagnetic plates that line the entire perimeter of a beam tube section. This material reduces the strength of all incident fields, and constructing an HOM damper from them is very straightforward. All HOM polarizations are damped due to their azimuthal symmetry. For these reasons, ferrite absorbers were chosen for the HOM couplers in the original R&D ERL – see Fig. 1.7[8, 9]. However, there are a few setbacks to this method of damping. Using ferrite tiles results in a reduced real-estate gradient (ratio of accelerating voltage to cavity string length), since they must be placed significantly far from the end cells to avoid damping the small amount of evanescent fundamental field that is present within the beam tube. This is evident from the length of the full cavity string (the 5-cell cavity along with beam tubes and ferrite sections), shown in Fig. 1.8. Also, ferrite heats up rapidly as it absorbs power, so a cooling circuit must be designed to minimize the heat load on the cavity. Due to these drawbacks, other damping schemes are actively being investigated for the BNL3 cavity.
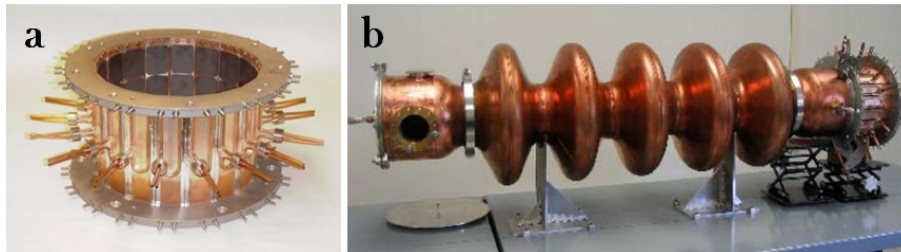
Figure 1.7: *a) Ferrite tile ring. b) Ring on ERL copper prototype.*

Coaxial Filter Couplers

Coaxial filter couplers consist of a pick-up electrode or loop that takes high-frequency RF power from the beam tube and transports it into a coaxial line to an RF dump out of the cryostat. The design must also provide an acceptable rejection of the fundamental mode, by including a high-pass RF filter that allows only HOM frequencies to pass through. These couplers are compact, and therefore don't have a large impact on cryostat size and design or beam
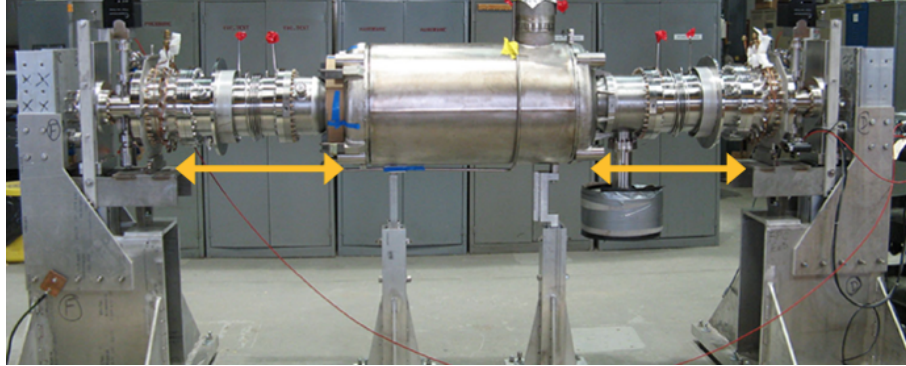
Figure 1.8: *The cavity string for BNL1. The 5-cell cavity is inside the central helium tank, and the ferrite sections are connected at the ends of beam tubes on each side.*

tube length. However, since they are typically placed on short beam tubes to maximize real-estate gradient, the design must also provide an acceptable rejection of the fundamental mode. The transmission profile is therefore very sensitive to detuning from resonance on these couplers. Furthermore, unlike the ferrite tiles which line the entire circumference of the beam tube, coax couplers are only capacitively (or inductively) coupled to a single azimuthal coordinate. As such, multiple couplers are required on each beam tube to ensure that fields from all HOM polarizations interact with at least one coupler. A coax filter coupler was designed and optimized for use with BNL3 and extensive measurement on a prototype has been carried out[10]. A schematic of this device is shown in Fig. 1.9, and a plot of the transmission is shown in Fig. 1.10.
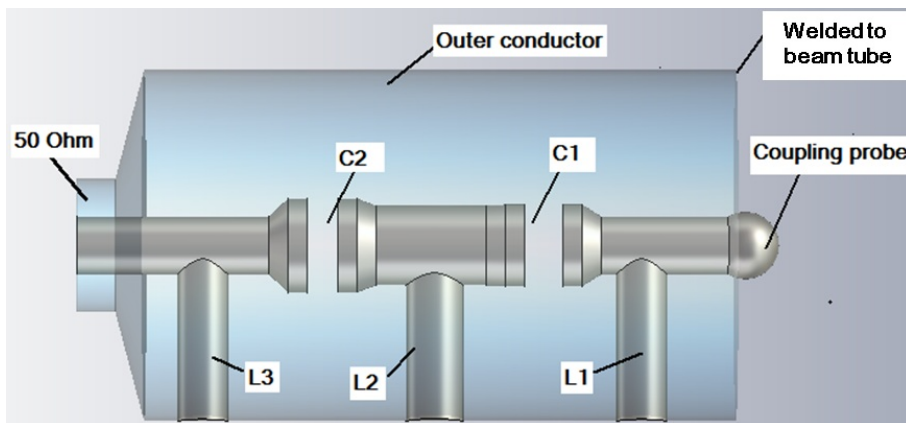
Figure 1.9: *Schematic of the BNL3 coaxial filter coupler.*
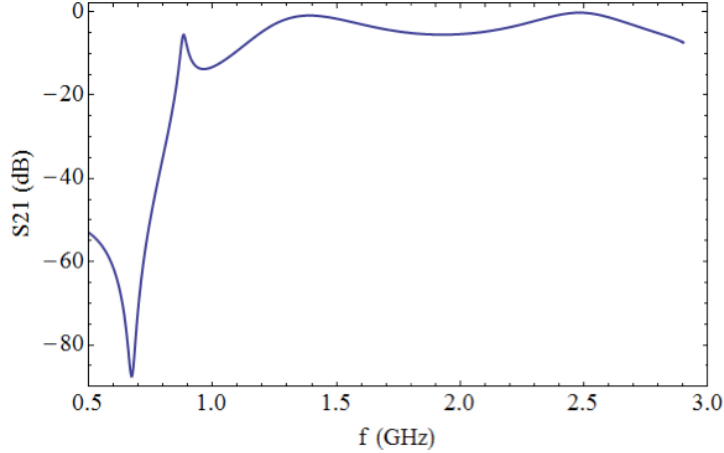
Figure 1.10: *Transmission of the BNL3 coaxial HOM coupler.*

Waveguide Couplers

The strongest advantages in using waveguides (WGs) as HOM couplers is that their shape offers a natural high-frequency cutoff which is easily selectable, and they require no tuning. They have a high power-handling capability and WGs of many different geometries are commercially available. Rectangular WGs have often been placed on the beam tubes of accelerator cavities in order to couple out HOM power, such as on the CEBAF cavity at JLAB shown in Fig. 1.11[11]. The ultimate drawback to using WGs is their comparatively large size, which in turn demands a large cryostat to accommodate them. The presence of the fundamental mode evanescent wave further complicates this issue, since the WG must be a few wavelengths long in order to keep the wave from reaching the RF load. And, as is the case for coax filter couplers, an arrangement of multiple WG couplers must be used to ensure the damping of all HOM polarizations.

1.3.3 Coupler Summary

A summary of the advantages and drawbacks of the 3 HOM coupler types is shown in Fig. 1.12. The main disadvantage of using WGs is the heat load added due to their large volume within the cryostat. However, modifying the WG geometry to reduce cryostat space represents an opportunity to make this method of HOM damping more practical. The next 2 chapters detail the design of a new WG HOM coupler utilizing a dual-ridge shape for volume reduction. Chapter 2 describes some early design considerations, and Chapter 3 gives the specifications of the finalized design which is suitable for prototype

Figure 1.11: *Waveguide HOM dampers on a CEBAF cavity at Jefferson Lab.*

fabrication and testing with the BNL3 copper cavity.

Coupler Type	Advantages	Drawbacks
Ferrite absorbers	Very little design required, good power handling capability, damps all mode polarizations	Reduced "real estate gradient" – requires long cavity string
Antenna couplers	Compact, offer excellent rejection of fundamental and good transmission of HOMs	Relatively expensive, sensitive to detuning from nominal frequency, inner conductor cooling challenges
Waveguide couplers	Qualitatively simple, requires no tuning	Large size within the cryostat

Figure 1.12: *Summary of the 3 HOM coupler methods.*

Chapter 2

Early Design Considerations for the BNL3 Waveguide HOM Coupler

This chapter summarizes the design goals of a waveguide HOM coupler for the BNL3 cavity in terms of both RF performance (power handling capability, transmission behavior) and geometry (volume within the cryostat, orientation of couplers). Several idealized models are described that serve to illustrate the motivation behind these goals. The culmination of these early studies resulted in a benchmark model, which is the topic of the next chapter.

2.1 Motivation

2.1.1 The Dual-Ridge Waveguide

In the past, WG HOM couplers have traditionally been rectangular in shape and attached directly to beam tubes, as shown previously in Fig. 1.11. The comparatively large volume of these HOM filters requires a large cryostat to contain them. This problem can be alleviated by changing the shape of the WG to reduce its overall volume, and one promising geometry is the dual-ridge waveguide. Fig. 2.1 shows the cross-sectional view of a dual-ridge WG along with its relevant parameters. The cutoff frequency for a dual-ridge WG structure decreases with center thickness g, and could therefore be made as small as desired[12]. It should be noted, however, that effective impedance also changes with g – an important consideration for matching. The result is a WG with an identical cutoff frequency as the rectangular shape, but with a much smaller cross-sectional area.
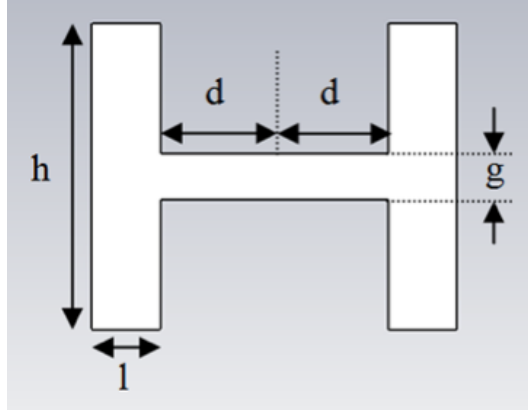
Figure 2.1: *Cross section of dual-ridge WG with relevant physical parameters.*

The electric field distributions of the lowest-order WG mode in both rectangular and dual-ridge WGs are shown in Fig. 2.2.
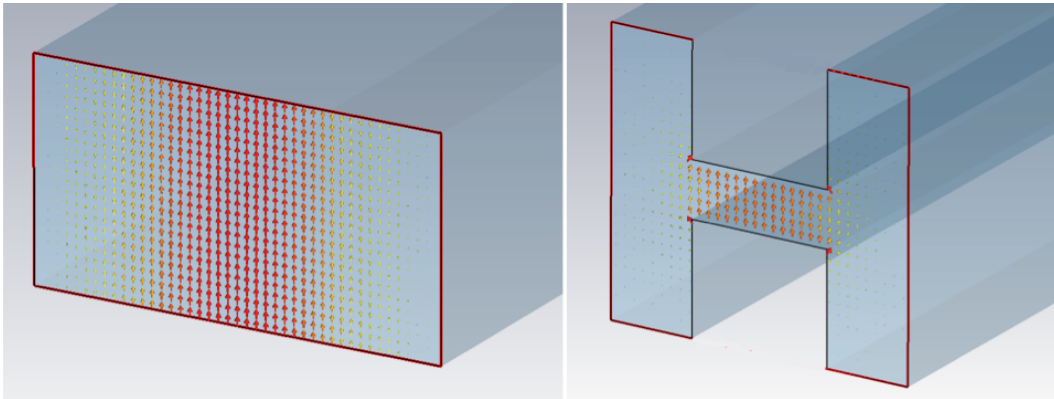
Figure 2.2: *Electric field distributions for the lowest-order resonance (left) a simple rectangular waveguide and (right) a dual ridge waveguide.*

2.1.2   Introducing a Transmission Line Connection

Even a relatively small dual-ridge WG demands a lot of cryostat volume when mounted directly on a beam tube and extending radially outward. Curving the WG is a possible solution to this problem, but isn't the most practical one in terms of a mechanical design. Alternatively, RF power from the beam tube could be coupled through a transmission line (namely, a coaxial line) to the WG. Incident power of all frequencies would therefore be introduced into the WG where frequencies above cutoff are transmitted through the WG to a load, while the fundamental frequency is attenuated. The main benefit with

14

this approach is the space-saving flexibility – no longer must the WGs jut straight out from the beam tube. Instead, by bending the transmission line or altering the coax-to-ridge connection, a design could be chosen that minimizes the overall volume needed for the entire set of WG HOM couplers.

A complication for this approach arises from the risk that an introduced coax-to-ridge transition can lead to power reflections. Several WG models of varying geometry were made in order to quantify, understand, and consequently minimize this effect. These simplified models are described in the following sections.

2.2   The Basic (Idealized) Model

The design strategy was to begin with the simplest possible model and slowly build in complexity. Even though using a dual-ridge WG was the ultimate goal, the additional parameters needed to characterize its shape were deemed unnecessary in the earliest stages. Instead, an ordinary rectangular WG was considered, containing an inner conductor (IC) running longitudinally in the center of the WG at one end and held in place by a conducting post. The model was envisioned to be a preliminary step to introducing a coaxial connection to a WG where the IC in the WG would in some way morph into the coaxial IC. The model is shown in Fig. 2.3, along with a comparison of its transmission with that of an empty WG of the same dimensions.
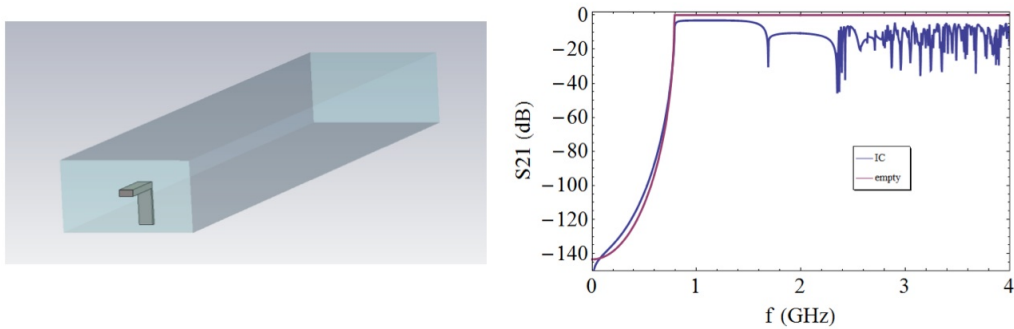
Figure 2.3: *Idealized WG model with inner conductor, and the power transmission through the structure.*

MWS was used to build the model and simulate its transmission. The space inside the WG is assumed to be vacuum and the power is transmitted and received through idealized ports at the WG ends. The cutoff region of the transmission profile for the IC model looks similar to that of the empty waveguide, but the distinction between the two becomes evident for $f > 1.5$ GHz.

15

Dips in transmission for the IC model occur as a result of resonances between the WG edges and introduced surfaces of the IC. Such dips in transmission are hazardous for an HOM coupler, since power from HOMs at these frequencies would not be effectively removed from the coupler. Instead, that power would drive resonances in the model leading to heating and other complications.

Many permutations of the model shown in Fig. 2.3 were made in an effort to understand the cause and reduce the occurrence of reflections. These included varying the IC geometry (including that of the IC support post), the IC support location, adding a second IC at the opposite end, and rounding the sharp IC edges. A small selection of these models is shown in Fig. 2.4.
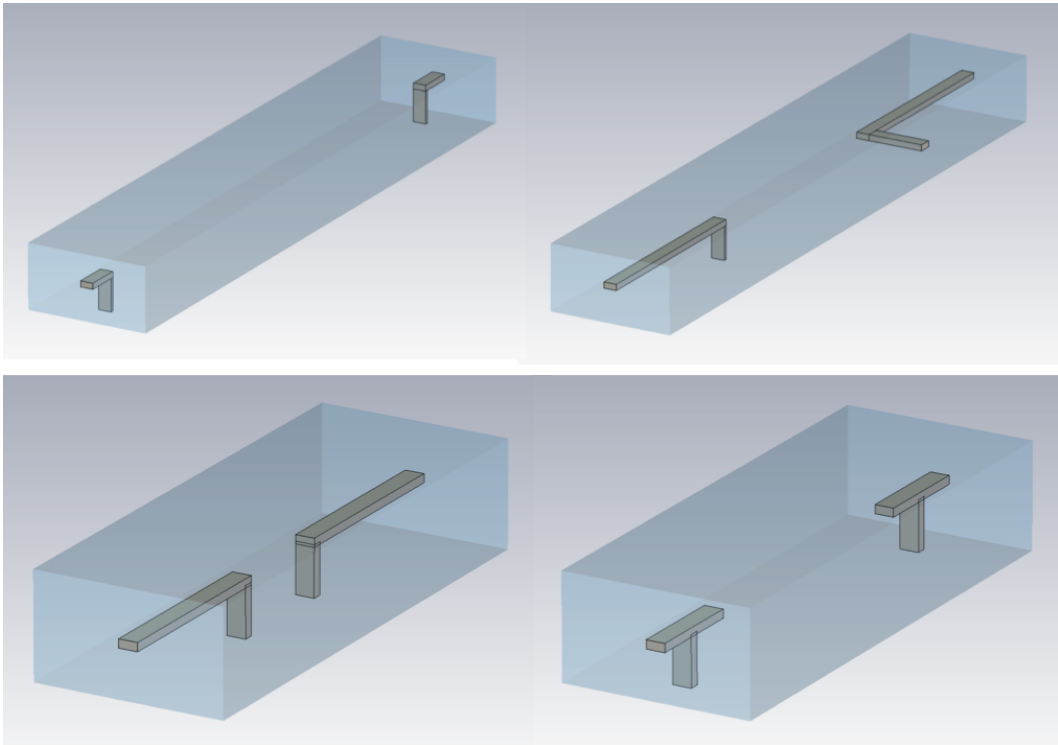
Figure 2.4: *Various idealized models with varying IC geometry and placement.*

Using the above criteria an improved version of this model was found and is shown in Fig. 2.5, which has good transmission (< 20 dB) at all frequencies below 3 GHz except for one dip near 1.545 GHz. The characteristic length for this resonance is 0.195 m, which is the distance from the end of the WG to the support post. This means that signals at this frequency, rather than traversing the WG, are instead powering resonances that occur between the conducting surfaces at the end of the WG and the support post. Then, moving the post closer to the WG end should shift the dip to the right. This is indeed verified by the model shown in Fig. 2.6.
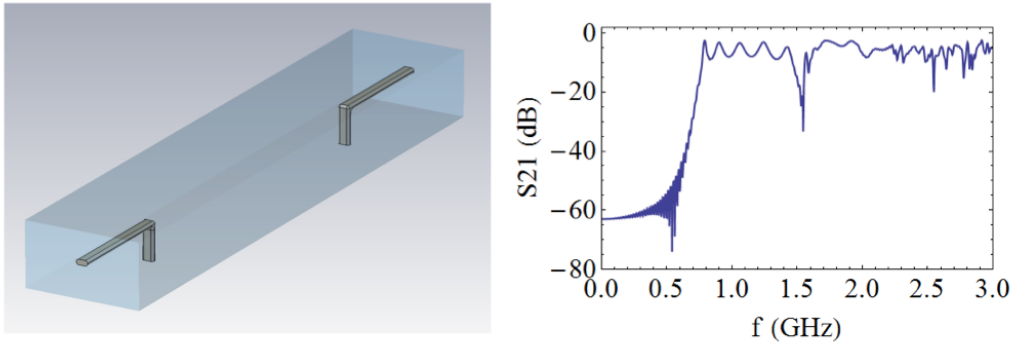
Figure 2.5: *Improved idealized model and its transmission.*
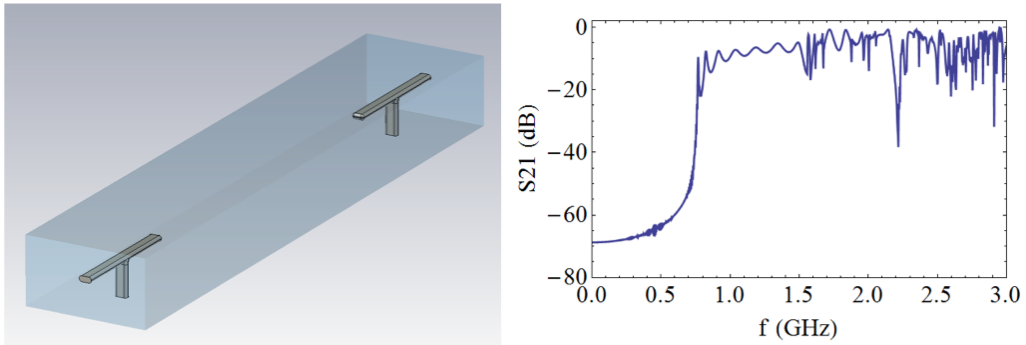
Figure 2.6: *Positioning the support closer to the WG end shifts the reflection to a higher frequency.*

From a transmission standpoint, the best model uses a combination of the previous 2, so that the reflections at 1.7 GHz and 2.3 GHz are "evened out". This is shown in Fig. 2.7.

These models don't suggest any breakthroughs in terms of HOM coupler design. They are far too simplistic in considering only rectangular WGs with no realizable connection for RF power transmission. However, they do give a modest glimpse at how the basic transmission behavior of a WG changes with the addition of conducting surfaces that complicate the boundary conditions. In the next section, models with a coaxial port are explored.

2.3 Addition of a Coax Port

A natural progression of the models listed above was to extend a coaxial line out of the WG end, as shown in Fig. 2.8. The outer conductor diameter was chosen to be 41 mm to match the beam tube ports on the BNL3 copper
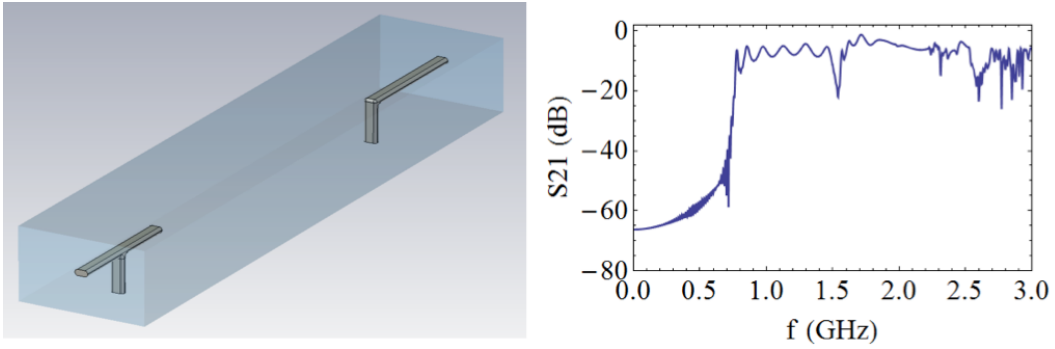
Figure 2.7: *Most successful idealized model and transmission.*

prototype.
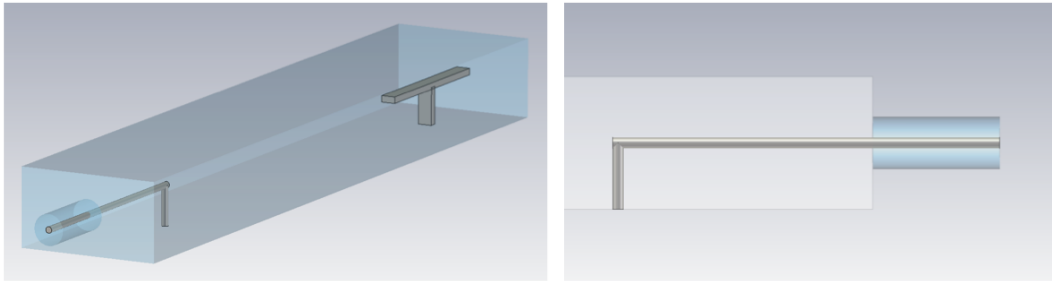
Figure 2.8: *Model with coax extension.*

While cutoff behavior near 704 GHz is acceptable for these models, there are still many reflection dips in the transmission at higher frequencies. In principle, this is caused in part by the impedance mismatch between the coaxial line and the WG. In order to minimize that effect, a "horn antenna" – a smooth transition between coax and WG outer conductors – was considered. This is illustrated in Fig. 2.9. In some cases, the IC was given a similar horn shape.
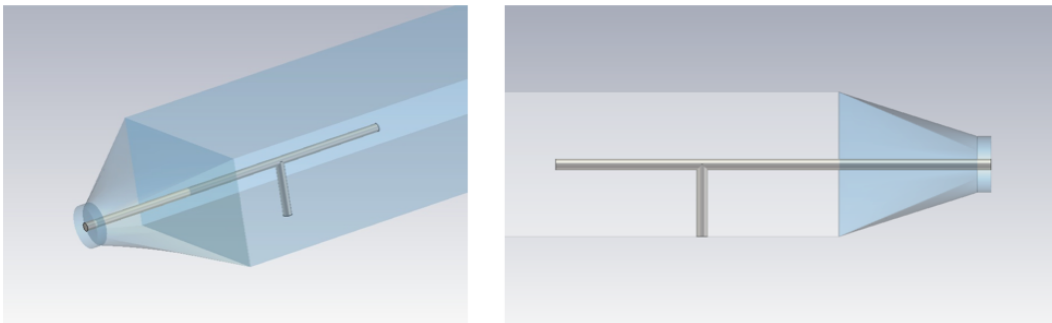
Figure 2.9: *Model with horn antenna.*

The most successful model made by incorporating a horn antenna was made

by placing the support for the IC within the horn region, as shown in Fig. 2.10. However, it should be noted that the transmission profile now resembles more closely a high-pass filter akin to a coaxial coupler rather than a waveguide. By adjusting the support post placement, the center frequency of the extreme dip near 700 MHz can be adjusted.
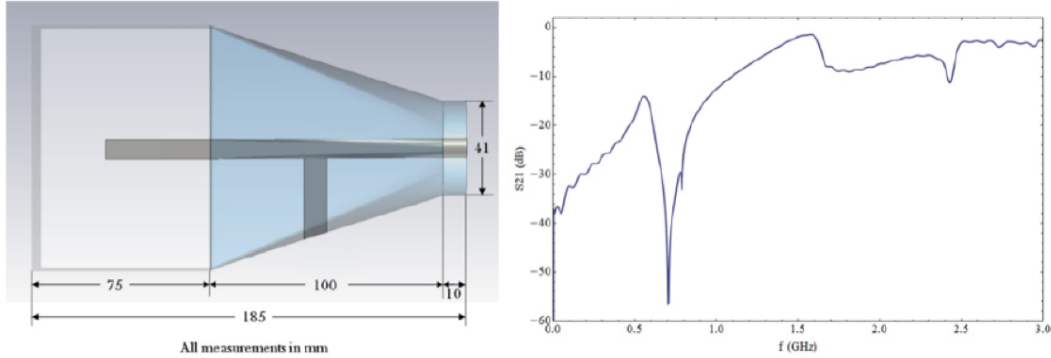
Figure 2.10: *Improved horn model and transmission.*

The high-frequency reflections have been almost completely removed from this model at least up to 3 GHz. However, the transmission behavior just above cutoff is unsatisfactory. Ideally, the behavior just above cutoff would replicate that of the empty WG shown in Fig. 2.3, where the difference between strongly attenuated signals and those transmitted are only separated by 50-100 MHz. Also, this model still doesn't represent the desired solution to HOM coupling for the BNL3 cavity, since it doesn't utilize a low-volume, ridge WG (a geometry that makes a horn transition much more complex).

Rather than coupling power into the WG end, requiring a bend in the coax to avoid couplers jutting radially outward, a perpendicular connection would be preferable. Such a connection was found to be more successful in terms of strong attenuation of the fundamental frequency along with consistent damping of HOM frequencies. It, along with an optimized dual-ridge WG geometry, are the subjects of the next chapter.

19

Chapter 3

Dual-Ridge Waveguide HOM Coupler Design for BNL3

This chapter summarizes the design of an HOM coupler for the BNL 3 cavity utilizing a perpendicular coax-to-ridge connection. The optimization steps leading to the final design are described, including 2 suggested ways of handling the HOM power carried by the coupler.

3.1 Design Basics

The TEM mode in a coaxial transmission line is more easily converted into the fundamental TE_{01} mode in a dual ridge WG rather than that in a rectangular WG. In a previous study to design a WG HOM coupler, this fact was utilized to export power out of a rectangular waveguide HOM coupler[13]. The so-called Broadband Waveguide to Coaxial Transition for High Order Mode Damping (BTHD) scheme used at the $DA\Phi NE$ accelerator consisted of a rectangular waveguide for filtering HOMs out of the beam tube, then incorporated a smooth transition from rectangular to dual-ridge geometry. The ridge shape allowed HOM power to then be converted into a coaxial TEM field and subsequently transferred to a load.

For the BNL3 WG HOM damper design, power must be carried in the opposite direction; that is, from the coaxial line into the ridged WG. But the requirements of the transition are the same: a junction that transfers as much power as possible with minimal reflection and without inducing any higher-order resonances discussed in Chapter 2. To find the best structure meeting this requirement, a starter dual ridge model was made with the appropriate

Table 3.1: Parameters for the initial dual-ridge WG model.

Param.	length (mm)
g	20
h	67
l	30
d	25
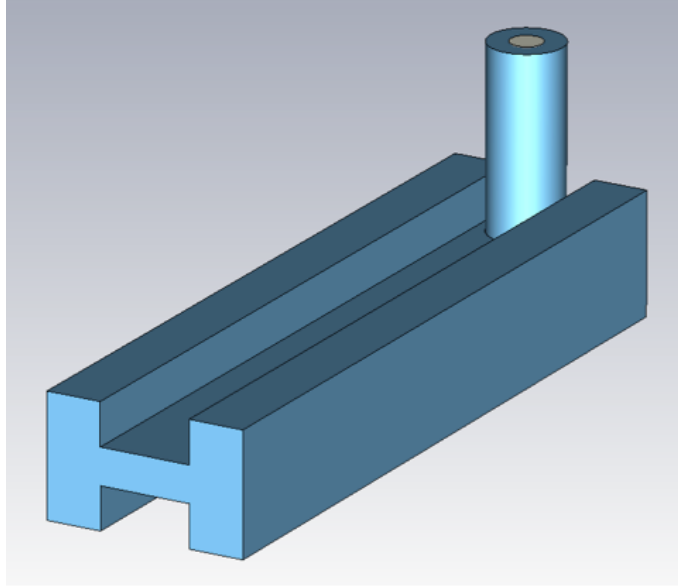
Figure 3.1: *Initial dual-ridge model in MWS.*

cutoff frequency, approximated by Ramo to be

$$f_c = \frac{1}{2\pi} \left(\frac{g}{\mu \epsilon h l d} \right), \tag{3.1}$$

where μ and ϵ are the permeability and permittivity of the WG medium, respectively, and g, h, l, and d are the physical parameters shown in Fig. 2.1[12]. These were selected not only to fit the appropriate cutoff, but so that the total volume of the WG was reasonably compact as a starting point. The initial parameters are given in Table 3.1. The model geometry is shown in Fig. 3.1.

Using this initial model, the optimization procedure was to first analyze the effect of coaxial line placement on S_{21} to determine its best location. Then, the WG parameters shown in Fig. 2.1 were optimized based on transmission characteristics and compactness.
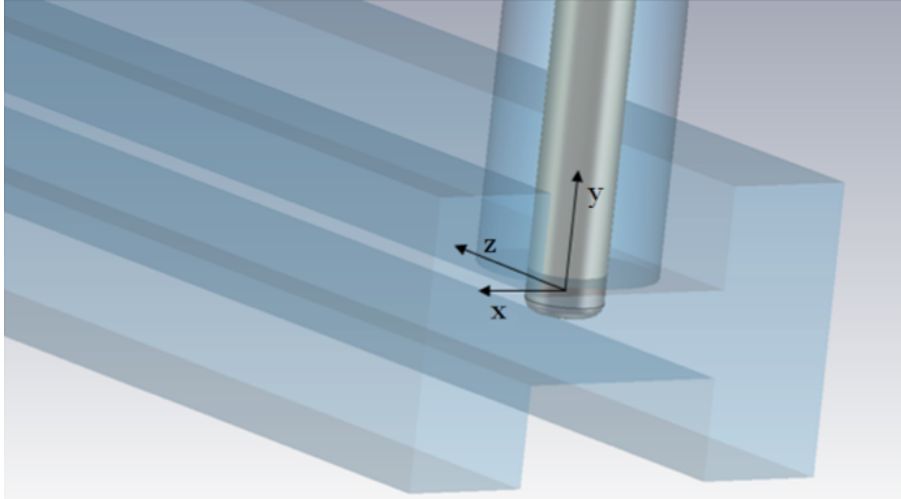
Figure 3.2: *Coordinates of the IC to be optimized.*

3.2   Optimization of the Coaxial Line

The free parameters involved in optimizing the coax line include the (x, y, z) coordinates of its placement as shown in Fig. 3.2, where x, y, and z refer to the location of the center point on the tip of the IC. The thickness of the inner conductor is also variable. The outer conductor diameter is fixed at 41 mm to match the BNL3 copper prototype cavity's port size. The shape of the IC tip could also be modified and optimized, but that wasn't a major focus of this study outside of smoothing the edges of the IC, which acts to reduce the effect of high frequency resonances. This is shown in Fig. 3.3. For the following models, rounding of the IC with $R = 2$ mm was used.

Fig. 3.4 shows a comparison of the transmission for the fundamental WG mode in a 400 mm-long model by the longitudinal location of the coax. There are two significant regions to compare: the transmission just above cutoff and at higher frequencies.

S_{21} just above cutoff flattens out more abruptly for the models where the coax line is further from the WG termination. This indicates that less power at these frequencies is reflected when the coax enters the WG further from the end. If the coax is positioned near the conducting surface at the WG end, power radiating in that direction will strike the surface and return into the coax. Alternatively, with the coax positioned further down the length of the WG, the fundamental mode is able to form on both sides of the IC, making it more likely that more power is transferred from coax to WG, i.e. S_{21} is closer to zero. The overall change in S_{21} from the fundamental frequency to the first expected HOM at 820 MHz is given in Table 3.2.
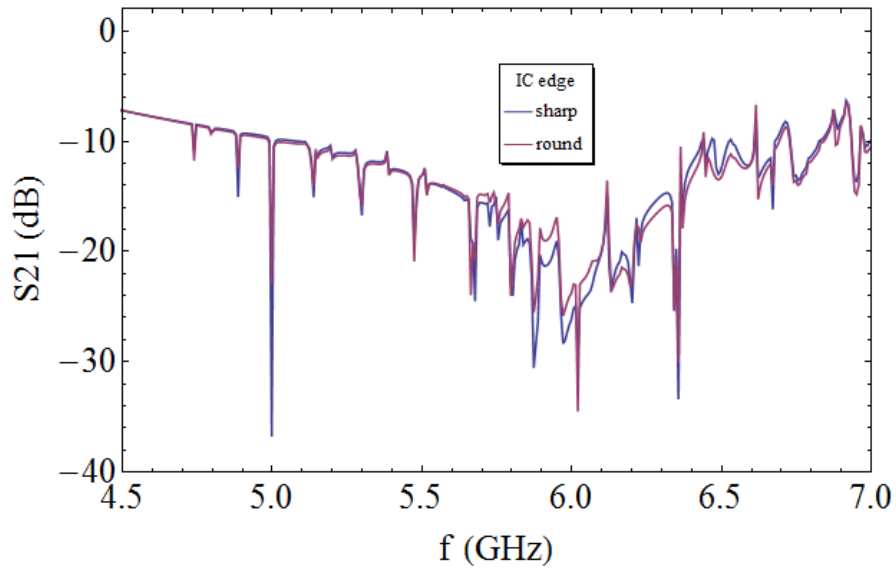
Figure 3.3: *The effect of rounding the IC edge on transmission.*
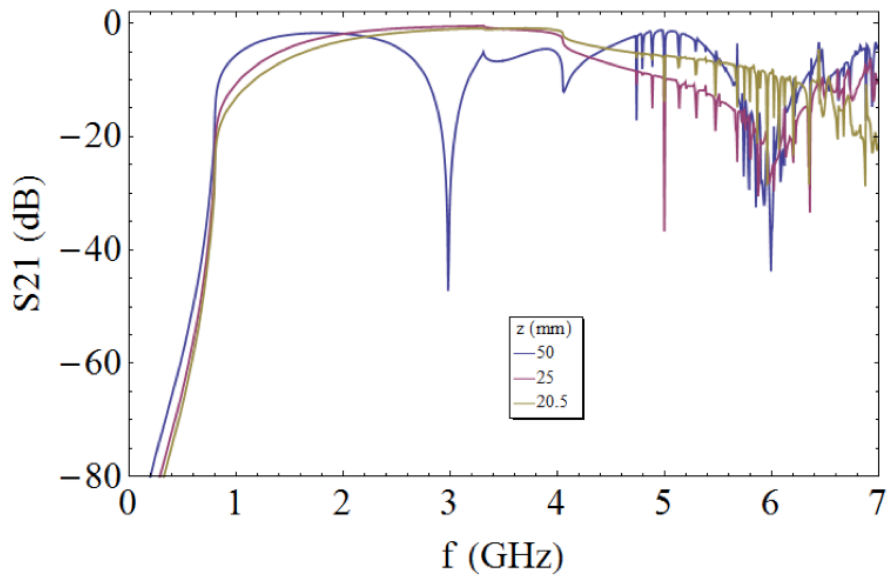
Figure 3.4: *Transmission comparison for models with different longitudinal IC placement.*

23

Table 3.2: Attenuation vs. longitudinal IC placement.

Coax z (mm)	Atten. (dB)
50	24.12
25	24.16
20.5	24.14

Table 3.3: Attenuation vs. IC penetration depth.

Coax z (mm)	Atten. (dB)
10	24.141
12	24.154
14	24.174
17	24.193
thru	21.694

While the difference in attenuation between the models isn't very great, the transmission for the model with a larger coax z is preferable since S_{21} is better (closer to 0 dB) at 820 MHz. The expense of this, however, is a resonance occurring between the WG end and the IC. For the $z = 50$ mm model, this resonance occurs near 3 GHz, a frequency that is excited because the distance between the IC and the conducting boundary of the WG corresponds to half the wavelength of a 3 GHz oscillation. By moving the coax closer to the WG end, this resonance can be pushed to a higher and higher frequency as desired, which is indicated in Fig. 3.4. The upper limit value is obtained by placing the coax at the end of the WG, where $z = 20.5$ mm. This value was selected for further simulation and optimization of subsequent models.

Next the effect of altering the IC penetration depth on transmission was analyzed. A comparison of various depths is shown in Fig. 3.5. As stated above, $g = 20$ mm for this model. A similar tradeoff is evident here as in Fig. 3.4: transmission for models with a larger penetration depth is successively better immediately above f_c, but generally worse for higher frequencies. Again, the overall change in S_{21} is not much different for the models, although it is trending upwards with a deeper penetration, as shown in Table 3.3. An exception is for the "IC thru" case, where the attenuation suffers, but the flattened S_{21} directly above cutoff is beneficial.
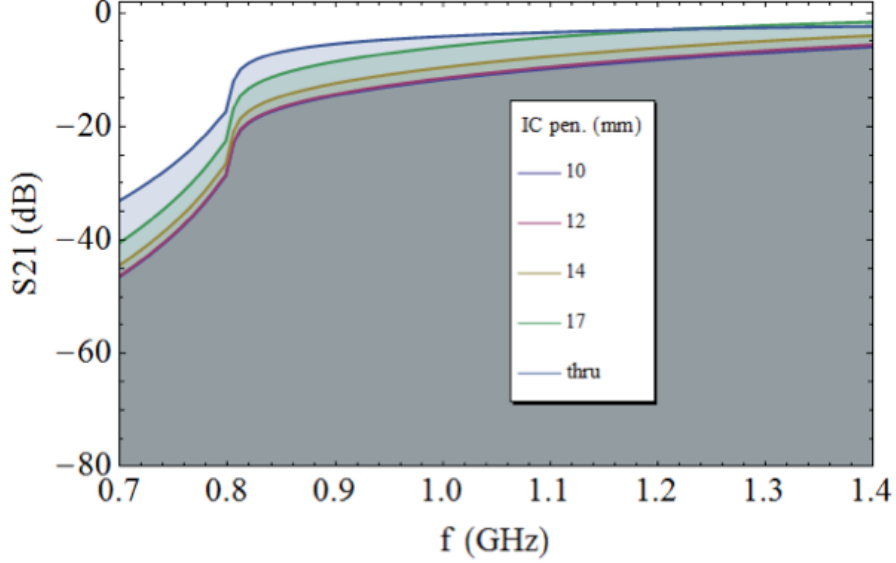
Figure 3.5: *Transmission vs. IC penetration depth.*

3.3   Optimization of the Waveguide Geometry

Since the waveguide geometry parameter g is the only parameter shown in Fig 2.1 that is directly proportional to f_c, it was chosen as the starting point for optimization. Fig. 3.6 shows a comparison of transmission of the starter model with varying g. In order to maintain the same cutoff frequency, the other parameters were each modified very slightly.

The S_{21} behavior just above cutoff is comparable for the three models – the attenuation for each in the frequency range between 720-820 MHz is given Table 3.4. However, transmission behavior improves at higher frequencies as g decreases. This is fortunate, since a successful WG coupler must be as compact as possible, and minimizing g while maintaining f_c necessarily means that the other parameters must be reduced as well due to the form of the equation for cutoff frequency. The danger in reducing g too much is an increased risk of field emission for smaller structures. (That can be better understood by using a dedicated eigensolver run of MWS with the WG attached to the BNL3 model – see following section). With this in mind, the limit of minimizing g was decided to be 1 cm.

Next, various combinations of h and l were studied (while keeping g and d fixed). The results for two models are shown in Fig. 3.7. The $h = 67$ mm, $l = 15$ mm geometry was determined to be the optimal choice for S_{21} considerations, and the reason for this is exemplified in Fig. 3.7 – better transmission at higher frequencies. These dimensions also allow the WG to be nearly square
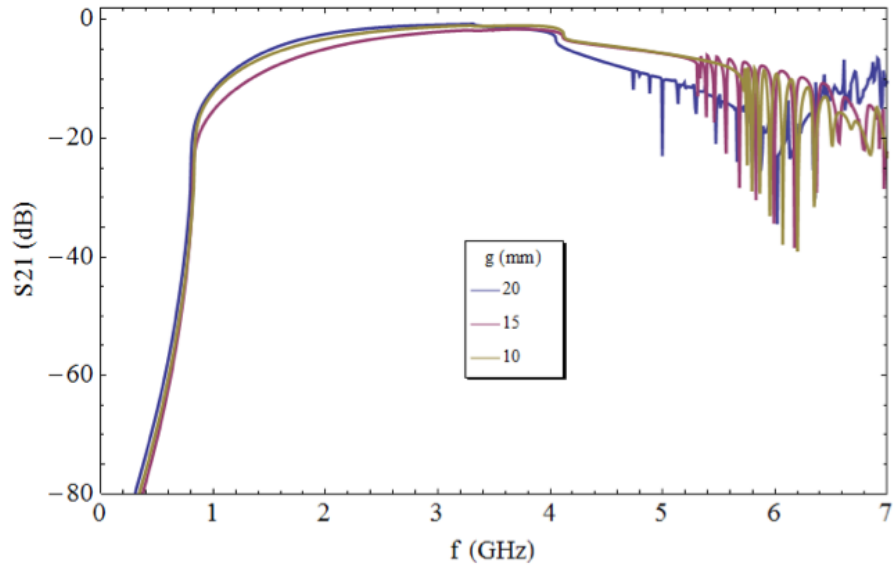
Figure 3.6: *Transmission vs. varying g.*

Table 3.4: Attenuation vs. length of *g*.

g (mm)	Atten. (dB)
20	24.14
15	24.42
10	24.77
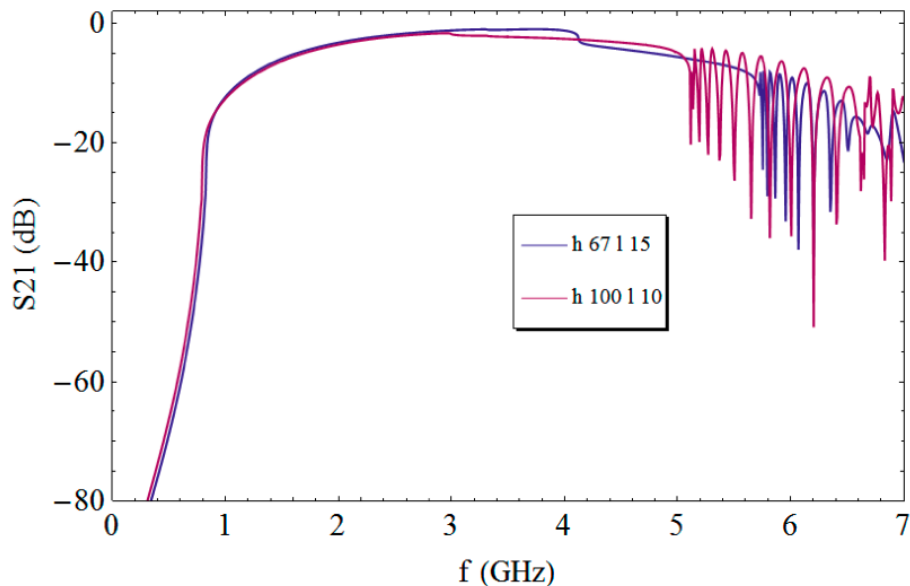
Figure 3.7: *Transmission vs. varying h and l.*

in terms of outer dimensions, and no section of it is greater than 15 mm thick, which is preferable for cooling. The parameter d was not methodically optimized, since its value of 25 mm allowed enough space for the coax to be brought off center to improve higher-frequency transmission.

3.4   The Benchmark Model

The best model after optimization is shown in Fig. 3.8, and a comparison of its cross-sectional volume with a rectangular WG of the same cutoff is shown in Fig. 3.9.

The transmission of this model compares favorably with that of the coax filter coupler previously designed for the BNL3 cavity (as described in Chapter 1). A combined plot of the performance of both is shown in Fig. 3.10.

The transmission shown in Fig. 3.10 only takes into account the fundamental WG mode (which has the E-field shown in Fig. 2.2). However, different resonant patterns can be excited at higher frequencies. S_{21} for the first 6 these are shown in Fig. 3.11, along with a cross sectional views of the longitudinal E-field. In all cases, transmission is satisfactory above cutoff up to 6 GHz except the symmetrical second and third modes. The disproportionally transmission for these modes is due to their lack of strong fields in the coaxial section of the WG (meaning they won't likely be excited). The first WG is the most important to study since it alone propagates between cutoff and 2.2 GHz, the
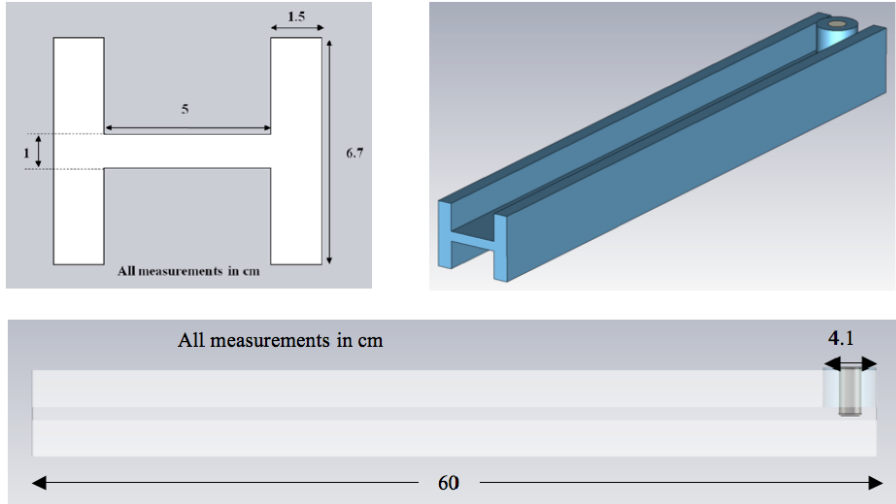
Figure 3.8: *Schematic for the benchmark model.*
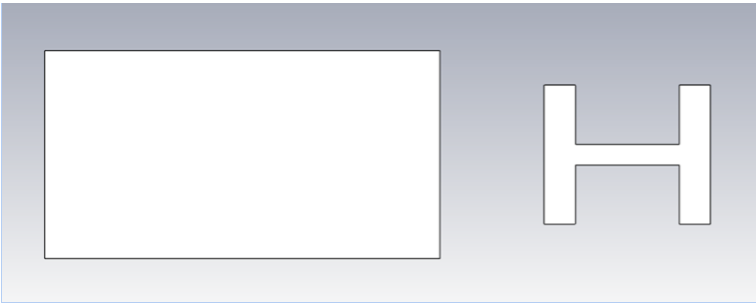
Figure 3.9: *Comparison of cross-sectional area of a typical rect. WG and the benchmark dual-ridge model, both with a cutoff frequency just above 704 MHz.*
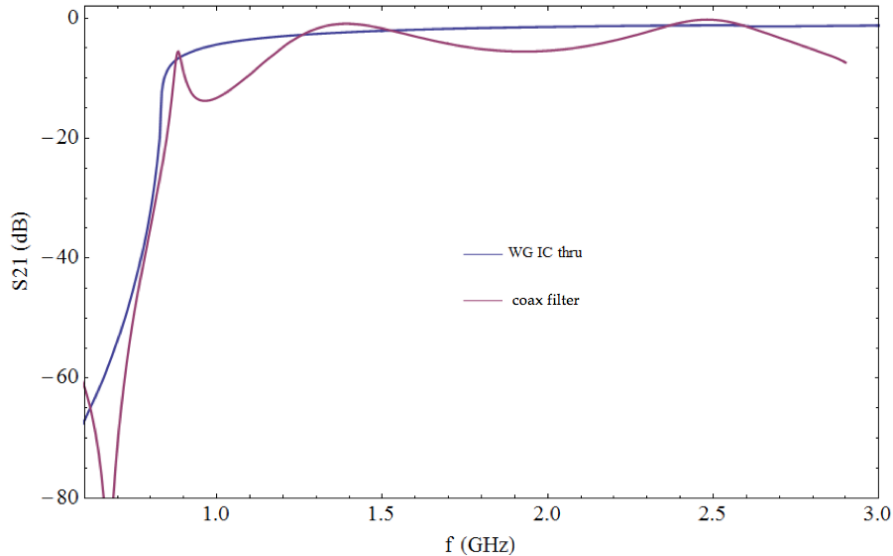
Figure 3.10: *Transmission comparison of benchmark model vs. the coax filter coupler design.*

frequency range where the most hazardous HOMs are expected to occur since the likelihood of BBU is inversely related to frequency.

3.4.1 Attempts at Coupling Power Out of the Waveguide

The most straightforward design for coupling power out of the WG involves using an identical coax connection at the opposite end – the transmission for this model is shown in Fig. 3.12. There is an evident difference between the S_{21} of this model, which is now measured from coax port to coax port, and the previous one. The introduced oscillations in transmission are the result of a resonance cavity created in the WG by removing the idealized port at the far end and replacing it with a conducting surface. The outcome is a model where signals at some HOM frequencies have better transmission, while signals at other frequencies are worse. Overall, the average transmission is about the same. In order to quantify the actual effect of adding this second coaxial line, a dedicated study of the frequencies at which the potentially hazardous HOMs in the BNL3 cavity occur is needed. It is worth mentioning, however, that the attenuation at the fundamental frequency for the 2-coax model is improved over the previous model, as evidenced by a sharper rise in S_{21} just above 704 MHz.
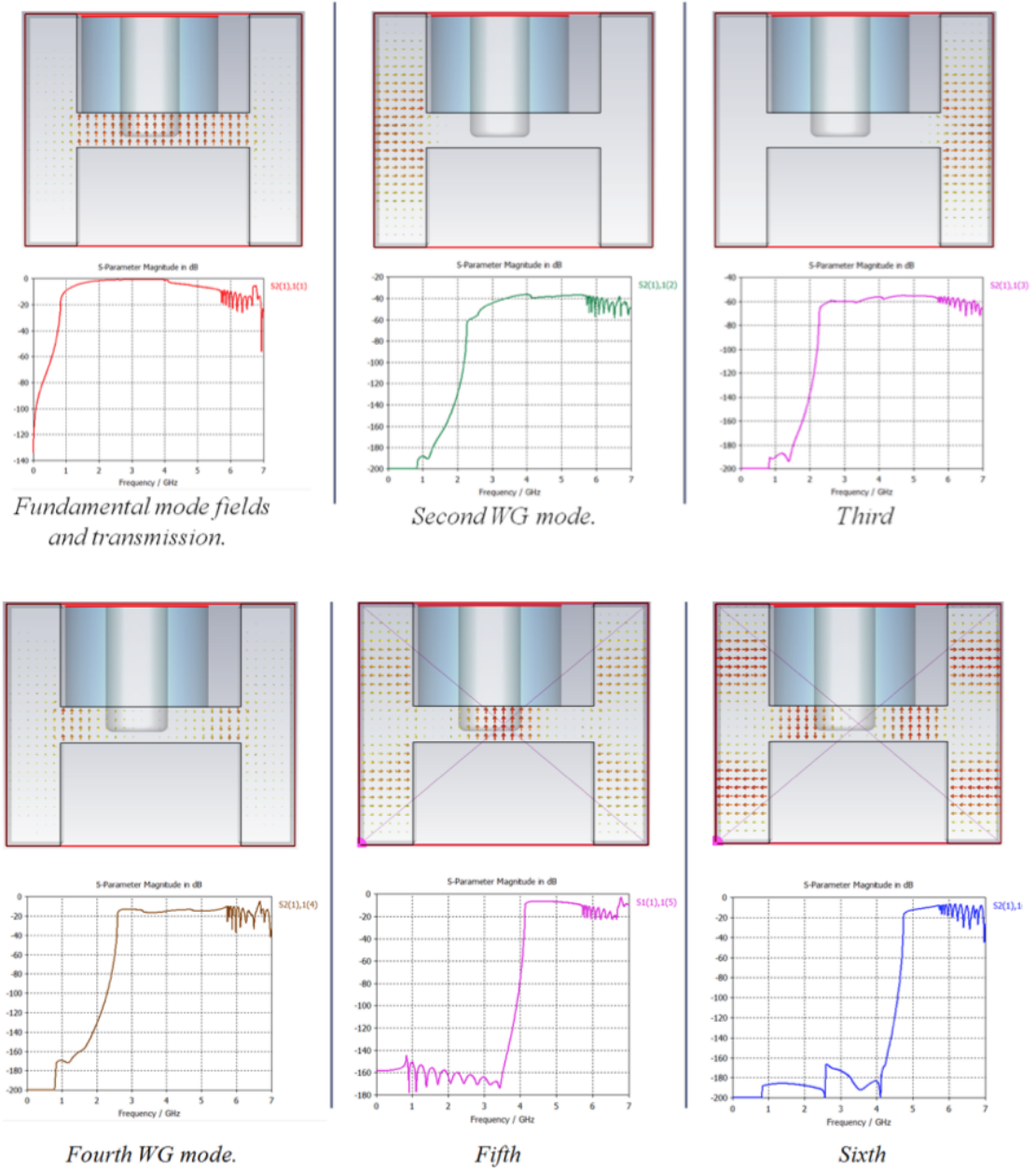
Figure 3.11: *Transmission and longitudinal E-fields of the lowest 6 WG modes through the coupler.*
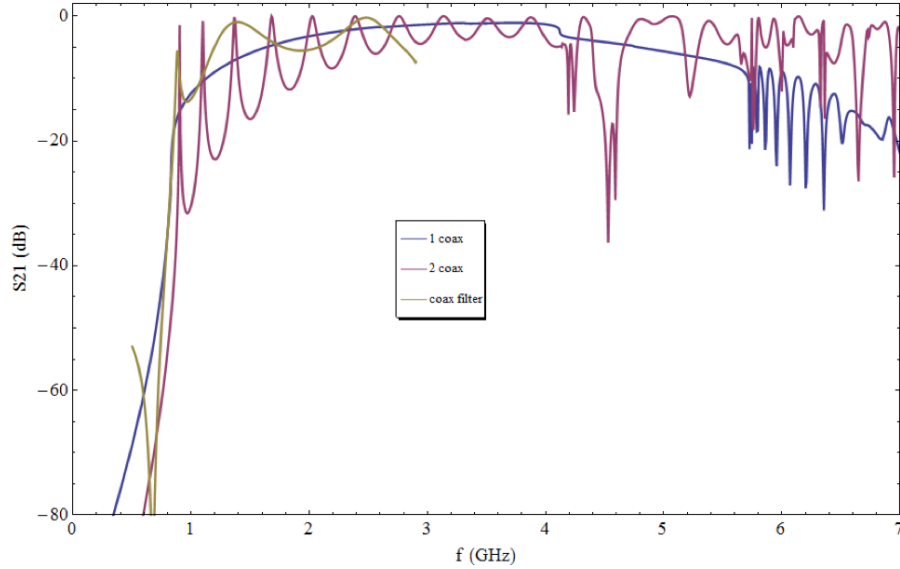
Figure 3.12: S_{21} *of the model with a coax at both ends, as compared with the single coax WG model and the coax filter coupler. (Note: the available coax filter data only goes up to 3 GHz.)*

3.4.2 Loaded WG Approach

An alternate solution to handling the HOM power is absorbing it in a WG load. This must be implemented carefully in a cryogenic system to avoid heating SC elements. By bringing a portion of the WG out of the liquid helium-filled region via a thermal transition, a load could be added to this section with designated cooling water or gas circuits. To this end, various load designs were studied by using a MWS model with a single port (on the coax) and simulating the reflected power, S_{11}.

The first load design consisted of a lossy metal "blade" in the center portion of the waveguide, as shown in Fig. 3.13. The motivation for this design is that, by introducing a small section of a lossy conductor in the plane where the E-field is max (for the fundamental WG mode), the resistance in the blade absorbs power from the signal. The long, slowly tapering shape ensures that reflections due to impedance mismatch are minimized.

The effect of the blade on transmission was unsatisfactory. Instead, using a ferrite-lined WG section was considered. Fig. 3.14 shows a MWS model of such a section, where all interior surfaces of the WG are covered with 3 mm of ferrite. The corresponding S_{11} is not a monotonically decreasing function above cutoff, which is an unexpected result. The cause of this was determined to be reflections off the protruding tiles. It is important to note that, in a phys-

31
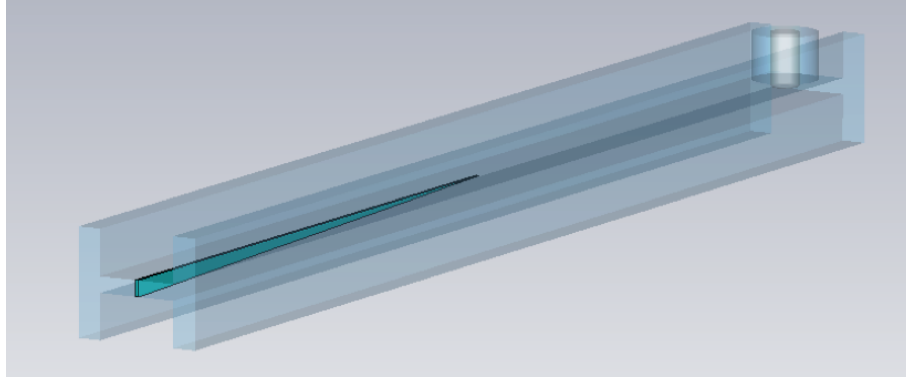
Figure 3.13: *Lossy metal "blade" HOM power load design.*
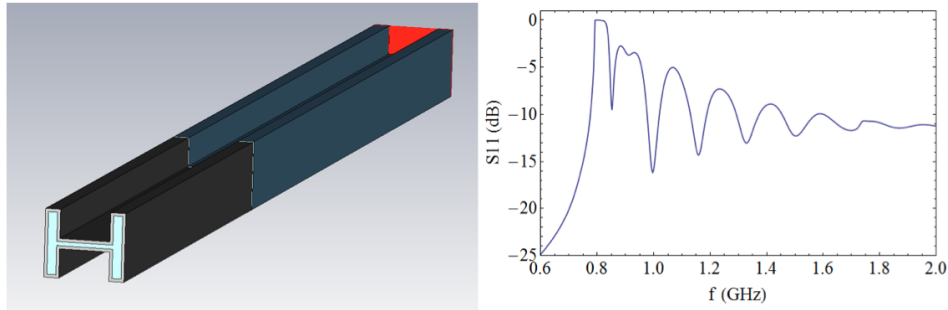
Figure 3.14: *Ferrite-lined WG section.*

ical system, the reflected power below the cutoff should be maximum ($S_{11} = 0$ dB), since any power coupled into the end of the WG below that frequency would be reflected. However, in Fig. 3.14 it is very small ($S_{11} \ll 0$ dB). This is an artifact of the MWS simulation. Below cutoff, the code attempts to excite a mode *within the cavity* that fails to propagate due to its frequency; there is no correspondence to any physical system for this. The same effect occurs in subsequent S_{11} plots. However, once the frequency reaches cutoff, S_{11} behaves normally, beginning at 0 dB and becoming more negative as frequency increases (depending, of course, on reflections).

A better solution combines the the ideas of the lossy blade and ferrite approaches, and utilizes 2 ferrite wedges in the center portion of the WG, as shown in Fig. 3.15. In this design, power in the first WG mode is reflected off the gradually sloping wedges, but in such a way that it remains in the center WG section and is eventually absorbed. This model was first analyzed without the coaxial transition, and the corresponding reflected power is shown in Fig. 3.16. As shown previously in Fig. 3.11, E-fields for the second and third-order WG modes would not be damped very well by these wedges since

32
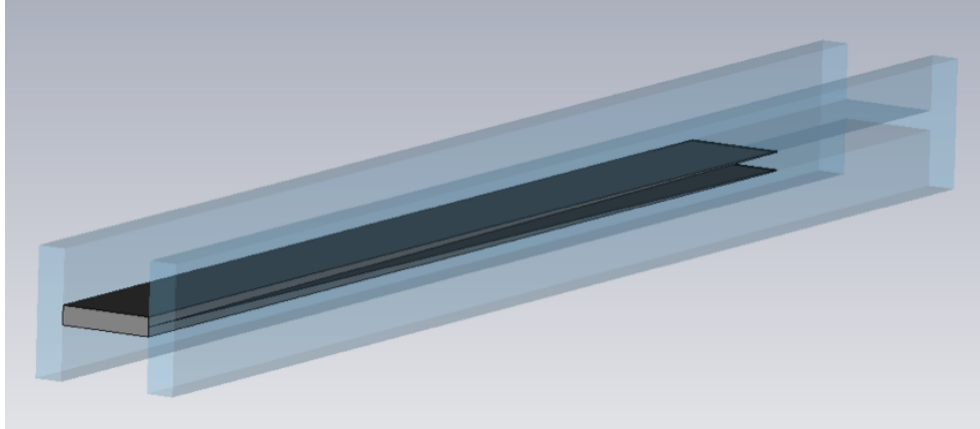
Figure 3.15: *Ferrite wedge HOM power load design.*
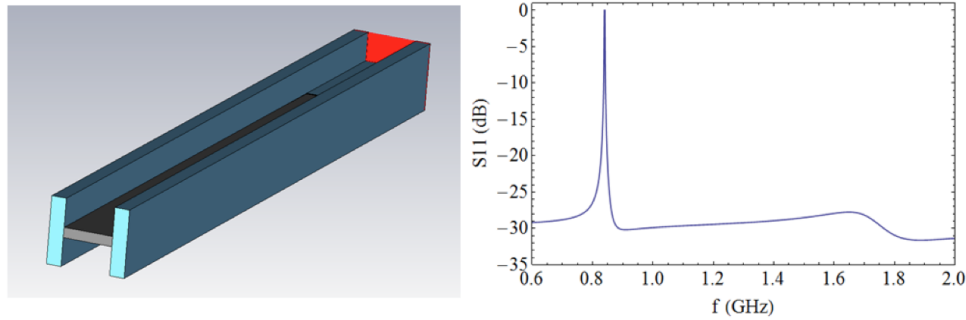
Figure 3.16: *Idealized ferrite wedge model (with no coax), and reflected power.*

their maximum fields occur in the side portions of the WG. If needed, similar wedges could be added to these regions.

As the frequency increases beyond cutoff, the power is rapidly absorbed; if $S_{11} = -30$ dB, only 0.1% of incident power is being reflected back out to the port. Of course this is an idealized case, and with the coax present the reflected power is much more prevalent, as shown in Fig. 3.17. This reflected power is best understood by observing the nonzero S_{21} in plots such as Fig. 3.10. For example, an S_{21} of -5 dB indicates only 32% of power being transferred across the coax-WG connection. As shown in Fig. 3.5, this effect can be controlled to some extent by changing the IC penetration depth; the "IC thru" case gives the least reflected power across the transition. Of course, the transmission of signals of all frequencies can be adjusted more or less uniformly in practice by changing the electrode's penetration into the beam tube; i.e. the penetration of the end IC which doesn't terminate in the WG. In this way, the ratio of transmission at HOM frequencies to that at the fundamental could be thought of as the most important figure of merit for an HOM coupler.
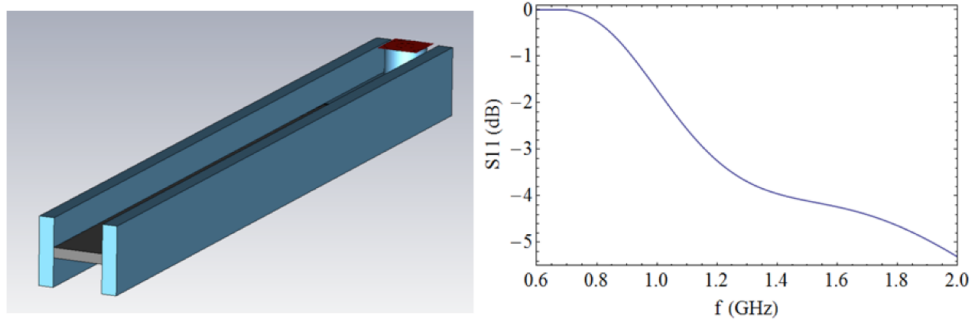
Figure 3.17: *Ferrite wedge model with coax added and the corresponding reflected power.*

3.4.3 MWS Study of Q_{ext} for HOMs

In order to more accurately simulate the performance of the coupler, calculating Q_{ext} (as shown in Equation 1.9) for many modes with the couplers present on a BNL3 model is necessary. For the fundamental mode, this calculation was conducted on a 1-cell MWS model of the BNL3 cavity, shown in Fig. 3.18. The reduced model was used to reduce simulation time.

By the equations in section 1.2.3, using the eRHIC parameter for the fundamental accelerating gradient ($V = 20 \frac{MV}{m}$) and $\frac{R}{Q}$ generated by MWS, Q_{ext} was calculated to be $1.424 \cdot 10^{11}$. This corresponds to a power of 1.257 W. Calculations of the HOM power expected in the BNL3 cavity operating at eRHIC conditions in section 1.2 estimated 1.3 kW per coupler (assuming 6 couplers per cavity), so this relatively small amount of fundamental mode power is acceptable.
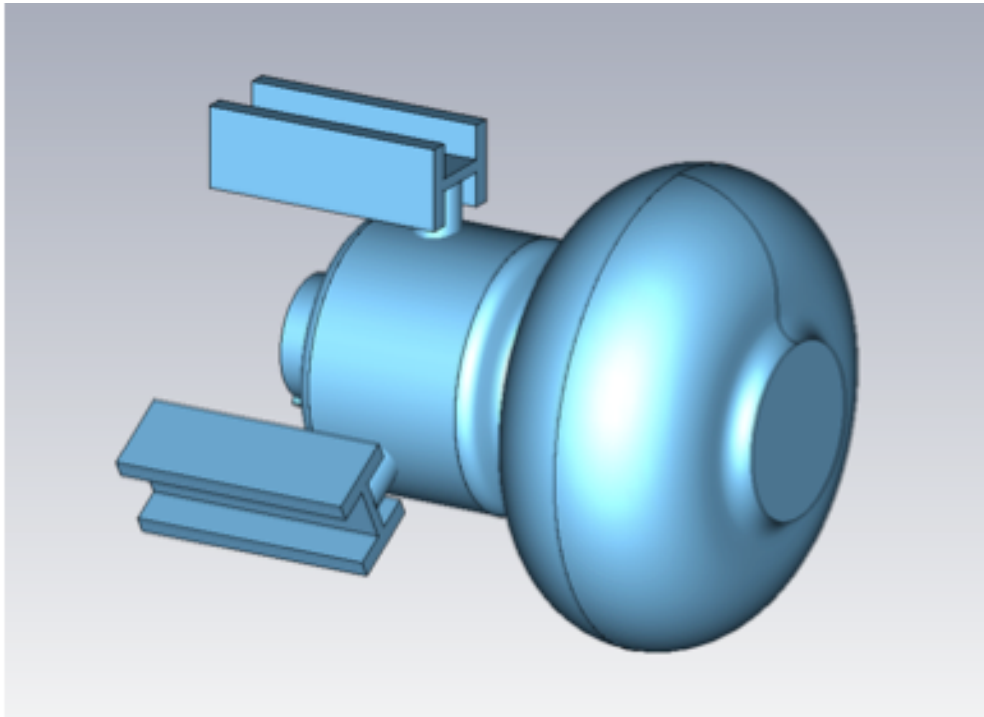
Figure 3.18: *Single cell BNL3 model used for fundamental mode Q_{ext} measurement.*

Chapter 4

Bead-Pulling Analysis of the BNL1 Prototype Cavity

This chapter presents recent HOM measurements carried out on the BNL1 copper prototype using a "bead-pulling" technique – a method of moving a field perturbation throughout the length of the cavity and studying the field response for a given HOM frequency. A description of the bead-pulling assembly is given, as well as the basic science behind the technique and some HOM characterization results.

4.1 Perturbation Measurements

Much can be learned about HOM resonances in accelerator cavities through the use of simulation codes such as CST Microwave Studio. However, to properly understand HOM behavior, comprehensive measurement and the resulting correspondence with simulation codes are needed. In particular, differences between simulation and measurement make it possible to quantize the effect of construction errors.

Several methods exist to study and identify HOMs; one of the most common is the bead-pulling technique. This involves sending a small dielectric or conductive perturbation (the "bead") along a string through the cavity while measuring changes in amplitude (or phase) at a single frequency. To measure the field flatness (i.e. the relative strength of the accelerating mode in each cell), this measurement is taken on-axis and at the fundamental accelerating frequency. To study HOMs, however, off-axis measurements at higher frequencies must be taken. A bead-pulling setup was constructed on the copper BNL1 cavity to study unidentified, high-Q HOMs previously seen in the cryogenic ERL. Another motivation for this work was to develop a measurement rou-

tine for HOMs in preparation for similar study on the copper BNL3 prototype cavity.

4.1.1 The Slater Method

Understanding the frequency change resulting from the insertion of an object into a resonant cavity is central to the bead-pulling technique. The interpretation of this change in frequency for the identification of the local field strength and direction as well as the cavity interaction parameters is well known in the accelerator community as Slater perturbation method[14]. Theoretical expressions for the frequency change have been derived for simple perturbation geometries with a near complete list found in a technical report by L. C. Maier, Jr.[15]. If the perturbing object has known properties, then it becomes possible to also determine the interaction parameter $\frac{R}{Q}$[16]. Bead-pulling for HOM identification in the copper BNL1 cavity has been discussed previously[1].

The Frequency Shift

The perturbation method consists of measuring the frequency shift due to the insertion of a perturbing object. The shift is given by the expression involving the local electric and magnetic field strength,

$$\frac{\Delta\omega}{\omega_0} = -F_E \frac{\epsilon_0 EE'}{U} + F_H \frac{\mu_0 HH'}{U} \tag{4.1}$$

where ϵ_0 and μ_0 are the dielectric and magnetic constants of free space, U is the stored energy in the cavity, and F_E, F_H are geometry factors that quantify the coupling of the perturbation to the E and H fields, respectively. Metallic beads, shaped either as spheres or thin rods are readily available and produce the largest signal but don't distinguish electric and magnetic fields. Dielectric beads with unknown dielectric constant and metallic needles have to be calibrated for accurate measurements. The results quoted in this chapter were performed with thin, needle-like conducting cylinders, treated as prolate metallic ellipsoids, that are sensitive to the longitudinal electric field and relatively insensitive to the transverse magnetic field components.

4.2 Bead-Pulling Assembly

The bead-pulling assembly for the ERL copper model is shown in Fig. 4.1. The setup consists of a pulley-mounted driver motor that moves the perturbing bead on a dielectric string through the cavity, and X-Y translation stages for
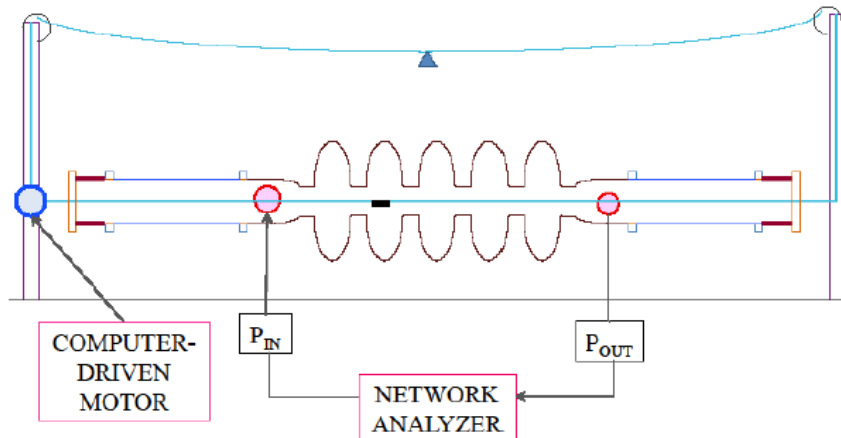
Figure 4.1: *Schematic of the bead-pulling assembly.*

precise on and off-axis alignment. A network analyzer supplies the power to excite resonant signals and detect the transmission. Coupling the network analyzer to a resonance can be achieved between the fundamental coupler and the pick-up probe, between capacitive probes entered in the end sections, or through small holes drilled into the cavity cells. It should be noted that the beam tubes of the copper prototype have been extended to match the length of the actual niobium ERL cavity in place. The MWS model used for analysis also meets those dimensions.

The induced phase shift for each HOM was obtained by taking the following steps. The network analyzer was set up to sweep across the desired HOM frequency. The resonance was centered, and the span set to 0. Then, to take a sweep measurement, the bead was sent through the cavity while the network analyzer measured the phase at the centered frequency. The timespan of this network analyzer measurement was set to coordinate with the time needed for the bead to traverse the cavity string. As the bead perturbs the cavity frequency by the relationship shown Equation 4.1, the phase is also proportionally perturbed. For HOM identification, quantifying this proportionality is not needed; only calculating the relative *phase change* for bead sweeps through different off-axis regions in the cavity is necessary. This is described further in the "HOM Analysis" section below.

Calibration and Field Flatness Measurement

As a preliminary measurement of the bead-pulling assembly, a field flatness measurement was taken and the result is shown in Fig. 4.2. Flatness is calculated by
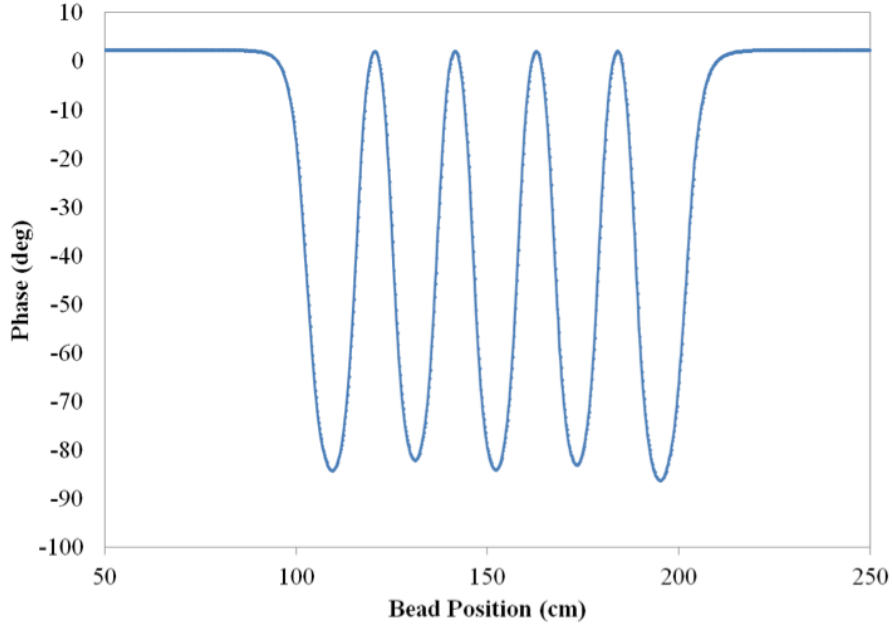
Figure 4.2: *On-axis field flatness measurement of the fundamental accelerating mode.*

$$Flatness(\%) = 100 - \left(\frac{\Delta\phi - \phi_{avg}}{\phi_{avg}} \right) \times 100, \qquad (4.2)$$

where ϕ_{avg} is the average of the phase offsets at the center of each of the 5 cells, and $\Delta\phi$ is the difference between the largest of these offsets and ϕ_{avg}. Field flatness was determined to be 97.16% for the data shown in Fig. 4.2. This agrees with previous measurements[1].

4.3   HOM Analysis

4.3.1   Measurements in the Dipole Group (800 - 1000 MHz)

In order to analyze the field structure of a given HOM, several off-axis bead-pull sweeps must be taken at different measurement angles. The result for such a measurement (taken 4 cm off-axis) is shown in Fig. 4.3 for the 958.92 MHz mode. This resonance was first observed in MWS simulation at 957.81 MHz as a "trapped" dipole without fields coupling into the beam tubes. All 5 cells are clearly visible in the plot, with the strongest coupling in the center
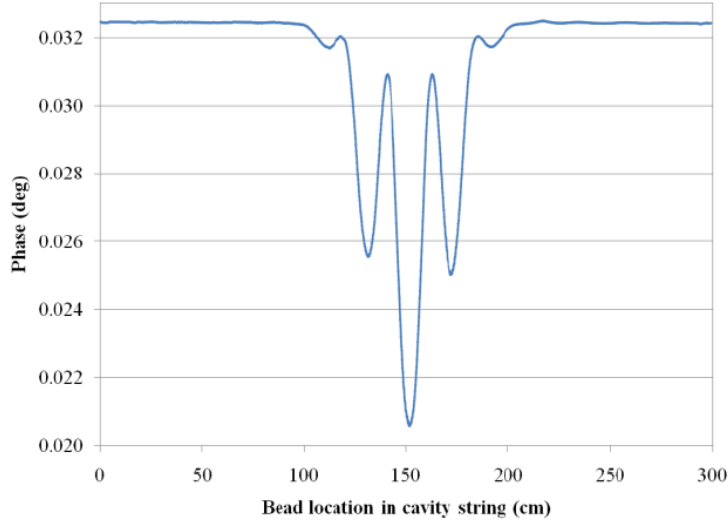
Figure 4.3: *Sweep data for the 958.92 MHz mode, as measured across the cavity.*

cell as expected for a trapped mode.

As noted in the equation above, the phase offset within a cell is directly related to the strength of E and H fields present and can be calculated by subtracting the maximum phase offset from the background (taken from a line fit to the outer points in Fig. 4.3 where the perturbation is not present in the cells). As the measurement angle changes, the maximum phase offset within a single cell correspondingly varies based on the HOM field structure, and this information can be used to identify the mode type (dipole, quadrupole, etc.). Fig. 4.4 shows how the phase offset varies with measurement (azimuthal) angle for sweeps taken at an equal radius for the 958.92 MHz mode. The phase offsets peak every 180°, indicating a clear dipole.

Another direct comparison can be made between the data and the MWS output to determine if the measured dipole is the same dipole mode solution given by MWS. As a post processing step, the longitudinal electric field for the MWS dipole was computed at a distance of 4 cm off-axis down the length of the entire cavity string. This distance corresponds to the bead-pull measurement distance, and the angle for the calculation was chosen as that of the maximum E-field plane. For a simple comparison, the measurement data (using the sweep data at an angle for maximum E, 180°) was scaled so that the center cell peak magnitudes were aligned, and the result is shown in Fig. 4.5. The relative field strengths in each of the 5 cells agree very well in this comparison, leading us to conclude that the measured mode and the MWS result are in fact the same dipole resonance.

40
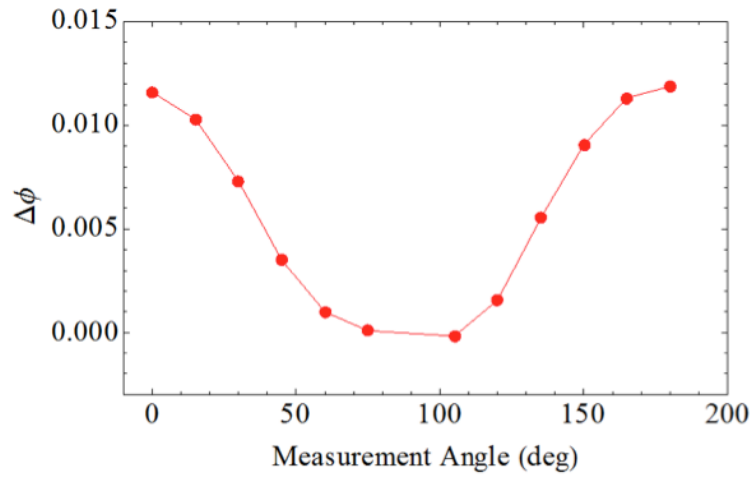
Figure 4.4: *Phase offset data for the 958.92 MHz HOM, showing dipole structure.*
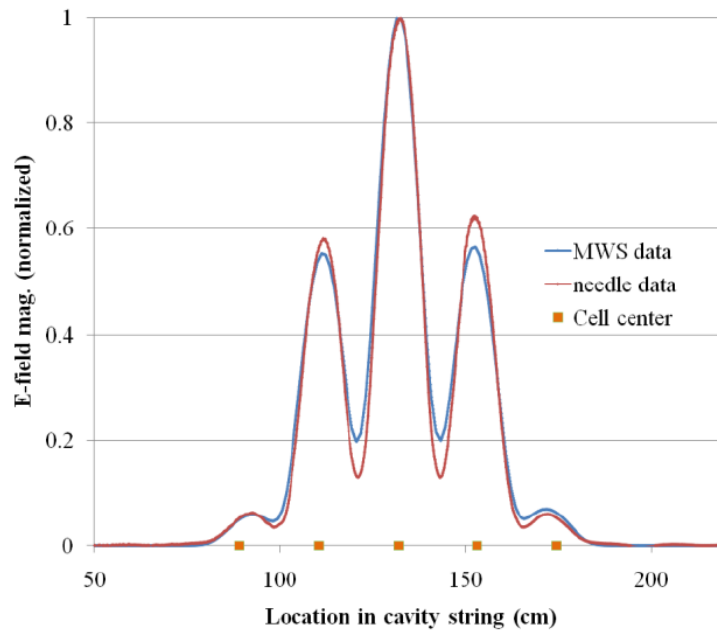
Figure 4.5: *Comparison of bead data and MWS output of normalized E_x for the 958.92 MHz HOM.*

41
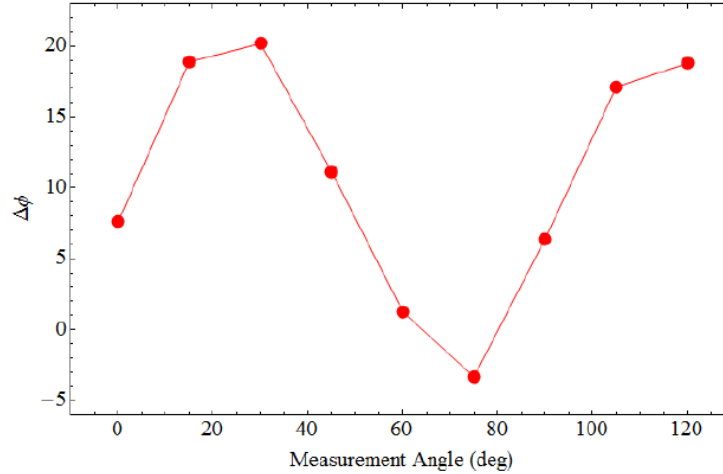
Figure 4.6: *Phase offset data for the 1.2189 GHz HOM, showing quadrupole structure.*

## 4.3.2 Bead Pull Measurements in the Quadrupole Group

Field structure for the 1.219 GHz mode was also measured using the bead-pulling technique. In order to sufficiently couple to the resonance, S_{21} was measured across the center cell and an adjacent cell. The phase offset result is shown in Fig. 4.6. From the plot, it is evident that the offset repeats every 90°, characteristic of a quadrupole mode.

The comparison of measured and MWS E-field magnitudes for this quadrupole is shown in Fig. 4.7. The relative E-field magnitudes in the cells do vary appropriately, but the correspondence isn't as clear as the dipole case discussed above. A possible reason for this disparity is that the bead-pull data wasn't taken at a measurement angle for maximum E-field (which would be closer to 25 °), while the MWS data is taken from this plane.

This quadrupole result matches that of a previous field structure measurement by an alternate method[7], where small conducting probes were placed in holes drilled in cavity walls. The holes are located 45° apart, near the cell apex. While keeping the excitation probe in one hole and successively measuring phase at the other 7, HOM structure was determined by counting the number of 180° phase jumps. All 5 resonances in the 1.215-1.24 GHz range were found to have 4 phase changes, indicating quadrupole structure. The result for the 1.2189 (1.22008 in the ERL) GHz mode for that measurement is shown in Fig. 4.8.
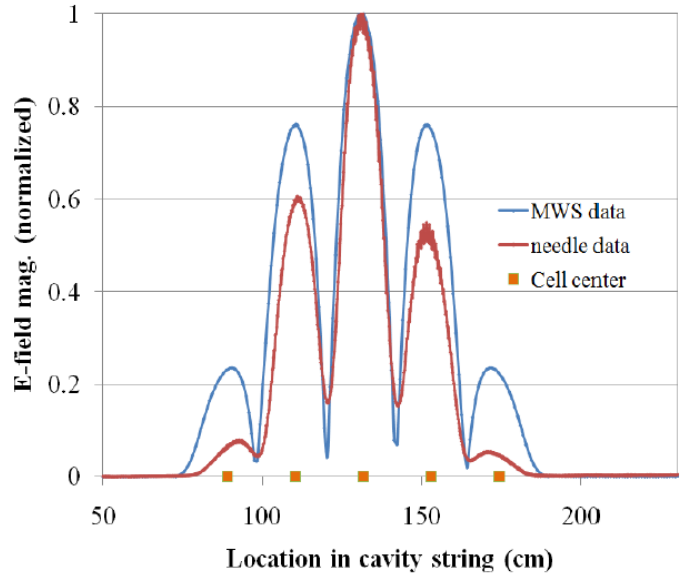
Figure 4.7: *Comparison of bead data and MWS output of normalized E_x for the 1.2 GHz HOM.*
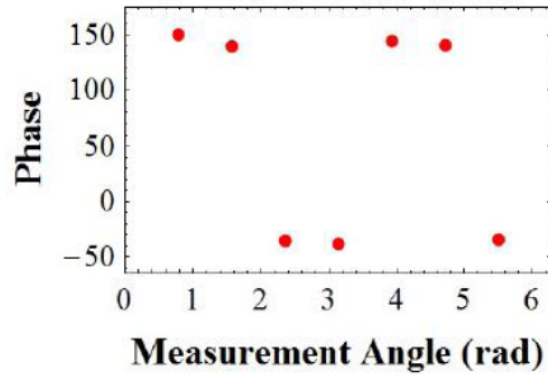
Figure 4.8: *Data for probe measurements on the 1.2 GHz HOM. There are 4 phase jumps of 180° as the measurement angle changes from 0° − 360°, indicating a quadrupole mode.*

Chapter 5

Conclusion

Higher-order modes present a danger to beam stability in accelerators and can result in excessive amounts of heat within a cryogenic system. In order to remediate these concerns, HOM couplers are used to transmit high-frequency power out of an accelerator.

Many design considerations factor into choosing the best HOM coupler for a specific application, such as compactness, the ability to handle necessary power loads, adequate rejection of fundamental mode signals, and commercial availability. An HOM coupler design for the next-generation ERL (BNL3) using a dual-ridge waveguide cavity was described. In terms of transmission, this coupler's simulated performance is comparable to a previously designed coaxial filter coupler. The dual-ridge geometry allows it to be a very compact structure, and connecting it to the beam tube with a coaxial transmission line allows a freedom of orientation to further reduce cryostat size. Finally, handling HOM power within the WG is a challenge for a cryogenic system. The two described solutions for this included adding a second, identical coaxial line to the far end of the waveguide or damping HOM signals with ferrite wedges in a section of waveguide extending out of the liquid helium vessel. The ferrite, which heats rapidly as it absorbs power, would need to be cooled by a water or a gas circuit.

In addition to designing a sufficient HOM coupler mechanism, characterizing the HOMs present in an accelerator is critical to determine if they pose a risk for beam break-up. One way to measure HOM fields is through bead-pulling – sending a small perturbation through an accelerator excited at a single HOM frequency and measuring the field response. A bead-pulling assembly was constructed on a copper prototype of the ERL (BNL1) cavity. It has been used to successfully characterize several HOMs, and measured results confirm those found with CST Microwave Studio. Further, the measurement routine devised to study these resonances can be immediately applied to an

identical bead-pulling assembly, soon to be set up on the BNL3 cavity.

Bibliography

[1] R. Calaga. PhD thesis, Stony Brook University, 2006.

[2] D. Kayran et al. Status of high current r&d energy recovery linac at brookhaven national laboratory. *Proceedings of 2011 Particle Accelerator Conference, New York, NY, USA THP006*. URL www.c-ad.bnl.gov/pac2011/proceedings/papers/thp006.pdf.

[3] I. Ben-Zvi, R. Calaga, H. Hahn, L. Hammons, E. C. Johnson, D. Kayran, J. Kewisch, V. L. Litvinenko, and Wencan Xu. Beam break-up estimates for the erl at bnl. *Proceedings of 2010 Particle Accelerator Conference, Kyoto, Japan*.

[4] Wencan Xu, I. Ben-Zvi, R. Calaga, H. Hahn, E. C. Johnson, and J. Kewisch. High current cavity design at bnl. *Nuclear Instruments and Methods in Physics Research Section A: Accelerators, Spectrometers, Detectors and Associated Equipment*, 622(1):17 – 20, 2010. ISSN 0168-9002. doi: 10.1016/j.nima.2010.06.245. URL http://www.sciencedirect.com/science/article/pii/S016890021001435X.

[5] H. Padamsee, J. Knobloch, and T. Hays. *RF Superconductivity for Accelerators*. Wiley-VCH, second edition, 2008.

[6] CST Microwave Studio. URL http://www.cst.com/Content/Products/MWS/Overview.aspx.

[7] E. C. Johnson, I. Ben-Zvi, H. Hahn, L. Hammons, and Wencan Xu. Higher order mode analysis at the bnl energy recovery linac. Technical Report BNL-96167-2011-IR, Brookhaven National Laboratory, 2011.

[8] H. Hahn, I. Ben-Zvi, R. Calaga, L. Hammons, E. C. Johnson, et al. Higher-order-mode absorbers for energy recovery linac cryomodules at Brookhaven National Laboratory. *Phys.Rev.ST Accel.Beams*, 13:121002, 2010. doi: 10.1103/PhysRevSTAB.13.121002.

[9] H. Hahn, E. M. Choi, and L. Hammons. Ferrite-damped higher-order mode study in the brookhaven energy-recovery linac cavity. *Phys. Rev. ST Accel. Beams*, 12:021002, Feb 2009. doi: 10.1103/PhysRevSTAB.12. 021002. URL http://link.aps.org/doi/10.1103/PhysRevSTAB.12. 021002.

[10] Wencan Xu, I. Ben-Zvi, S. Belomestnykh, H. Hahn, and E. C. Johnson. New hom coupler design for high current srf cavity. *Proceedings of 2011 Particle Accelerator Conference, New York, NY, USA*. URL accelconf. web.cern.ch/accelconf/PAC2011/papers/tup060.pdf.

[11] R. Rimmer et al. Waveguide hom damping studies at jlab. *HOM10 Conference, Ithaca, NY, USA*, 2009.

[12] Ramo, Whinnery, and Van Duzer. *Fields and Waves in Communication Electronics.* Wiley, second edition, 1965.

[13] R. Boni, F. Caspers, A. Gallo, G. Gemme, and R. Parodi. A broadband waveguide to coaxial transition for high order mode damping in particle accelerator rf cavities. *Particle Accelerators*, 45(4):195, 1994.

[14] L. C. Maier and J. C. Slater. Field strength measurements in resonant cavities. *J. Appl. Phys.*, 23:68, 1952.

[15] L. C. Maier. Field strength measurements in resonant cavities. Technical Report MIT-RLE-TR-143, MIT, 1949.

[16] H. Hahn and H. J. Halama. Perturbation measurement of transverse r/q in iris-loaded waveguides. *IEEE Trans. Microwave Theory and Techniques*, MIT-16:20, 1968.